RAYTHEON COMPANY
Research Division
131 Spring Street
Lexington, MA 02173

MMIC COMPENSATION NETWORK FOR PHASED ARRAY ELEMENT MISMATCH

K. Simon
J. Wendler
R. Pozgay
M. Schindler

Contract No. N00014-87-C-2517

Final Report

TASK I

RAY/RD/S-4248A

September 14, 1990

Prepared for

Naval Research Laboratory
4555 Overlook Ave., SW
Washington, DC 20375-5000
Code 6853

Contract No. N00014-87-C-2517
Contractor: Raytheon Research Division

RAYTHEON COMPANY
Research Division
131 Spring Street
Lexington, MA 02173

MMIC COMPENSATION NETWORK FOR PHASED ARRAY ELEMENT MISMATCH

K. Simon
J. Wendler
R. Pozgay
M. Schindler

Contract No. N00014-87-C-2517

Final Report

TASK I

RAY/RD/S-4248A

September 14, 1990

Prepared for

Naval Research Laboratory
4555 Overlook Ave., SW
Washington, DC 20375-5000
Code 6853

Contract No. N00014-87-C-2517
Contractor: Raytheon Research Division

Unclassified

SECURITY CLASSIFICATION OF THIS PAGE

REPORT DOCUMENTATION PAGE

1a. REPORT SECURITY CLASSIFICATION None	1b. RESTRICTIVE MARKINGS
2a. SECURITY CLASSIFICATION AUTHORITY	3. DISTRIBUTION / AVAILABILITY
2b. DECLASSIFICATION/DOWNGRADING SCHEDULE	
4. PERFORMING ORGANIZATION REPORT NUMBER(S) RAY/RD/S4248A	5. MONITORING ORGANIZATION REPORT NUMBER(S)
6a. NAME OF PERFORMING ORGANIZATION Raytheon Company Research Division 6b. OFFICE SYMBOL (if applicable)	7a. NAME OF MONITORING ORGANIZATION
6c. ADDRESS (City, State and ZIP Code) 131 Spring Street Lexington, MA 02173 Code 6853	7b. ADDRESS (City, State and ZIP Code)
8a. NAME OF FUNDING / SPONSORING ORG. Navai Research Laboratory 8b. OFFICE SYMBOL (if applicable)	9. PROCUREMENT INSTRUMENT IDENTIFICATION NUMBER Contract No. N00014-87-C-2517
8c. ADDRESS (City, State and ZIP Code) 4555 Overlook Ave., SW Washington, DC 20375-5000	10. SOURCE OF FUNDING NUMBERS PROGRAM ELEMENT NO. / PROJECT NO. / TASK NO. / WORK UNIT ACCESSION NO.

11. TITLE (include Security Classification)
MMIC COMPENSATION NETWORK FOR PHASED ARRAY ELEMENT MISMATCH

12. PERSONAL AUTHOR(S)
K. Simon, J. Wendler, M. Schindler, J. Pozgay

13a. TYPE OF REPORT	13b. TIME COVERED	14. DATE OF REPORT (Year, Month, Day)	15. PAGE COUNT
Final Technical	FROM 10/87 TO 6/88	1990 September 14	73

16. SUPPLEMENTARY NOTATION

17. COSATI CODES		
FIELD	GROUP	SUB-GROUP

18. SUBJECT TERMS (Continue on reverse if necessary and identify by block number)
Antenna Input Mismatch, Tuning Scheme, MMIC Compatible, Notch Radiator

19. ABSTRACT (Continue on reverse if necessary and identify by block number)

A tuning scheme has been developed that compensates the radiating element input mismatch that occurs in broadband phased arrays. The compensated radiator has an input VSWR less than 2.0 from 8 to 18 GHz and antenna scan angles from 0° to 60°. Keywords: PHASED ARRAYS; BROADBAND. (RH)

20. DISTRIBUTION / AVAILABILITY OF ABSTRACT ☐ UNCLASSIFIED / UNLIMITED ☐ SAME AS RPT. ☐ DTIC USERS	21. ABSTACT SECURITY CLASSIFICATION
22a. NAME OF RESPONSIBLE INDIVIDUAL Dr. Charles Young	22b TELEPHONE (Include Area Code) (202) 767-3008 22c OFFICE SYMBOL Code 6854 ES&TD

DD FORM 1473, 84 MAR 83 APR edition may be used until exhausted. All other editions are obsolete.

SECURITY CLASSIFICATION OF THIS PAGE

Unclassified

TABLE OF CONTENTS

TABLE OF CONTENTS (Continued)

LIST OF ILLUSTRATIONS

LIST OF ILLUSTRATIONS (Continued)

LIST OF TABLES

1.0 INTRODUCTION

1.1 Program Statement

This program, "MMIC Compensation Network for Phased Array Element Mismatch", studied various MMIC compatible methods of compensating the radiating element input mismatch that occurs in broadband phased arrays. The radiating element input mismatch is due to mutual coupling between radiating elements. This input mismatch varies with frequency and antenna scan angles and may be as high as 3.8:1. The power amplifier for the radiating element requires a good match (generally better than 2:1) for optimal performance. A circulator would normally be used in such a mismatch situation but conventional circulators are too large for typical phased array element to element spacing and may also be too heavy for air- and space-bourne systems (miniature circulators are still in development). Therefore, some other methods of compensating the radiating element input mismatch need to be investigated.

to Form 1473

1.2 Program Goal

The goal of this program was to find an MMIC compatible method of compensating the radiating element input mismatch that occurs in broadband phased arrays. Table 1-1 lists the system requirements that the compensated antenna radiator must satisfy. A compensating network would be considered worthwhile if the compensated radiator satisfies the system requirements and if the improvement in radiator performance (gain) is greater than the losses caused by the compensating network.

A notch radiator was the assumed radiating element used throughout this program. Figure 1-1 shows an exploded view of a notch radiator. The input line is stripline. The ground plane on either side contains notches formed by tapered slotlines. Energy is coupled to the notches by a perpendicular intersection

PSN-87-1340

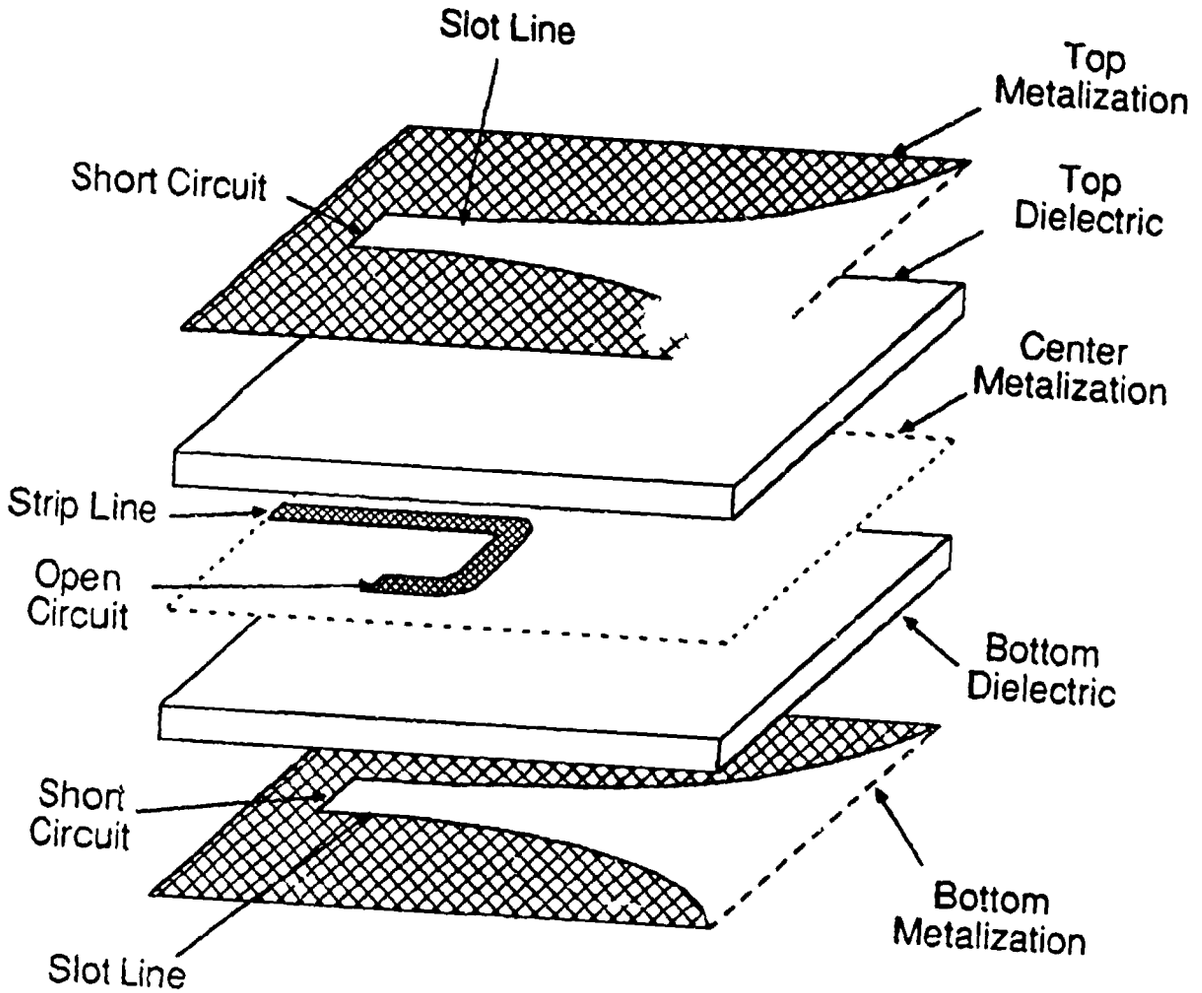

Figure 1-1. Fully Exploded View of a Notch Radiator.

of the stripline and slotlines. The stripline is terminated by an open circuit and the slotlines are terminated by short circuits. These system requirements and antenna properties governed the compensating network study.

Table 1-1
System Requirements

Frequency of Operation	6 - 18 GHz
Instantaneous Bandwidth	500 MHz
Radiating Element Input VSWR	< 2.0:1
Antenna Scan Angle	0 - 60°

Based on these system requirements, certain antenna properties were assumed. The assumed antenna properties are listed in Table 1-2.

Table 1-2
Antenna Properties

Element Type	Notch Radiator
Number of Elements*	1000 - 6000
Configuration	Planar

* Each element controlled by its own transmit/receive (T/R) module

2.0 SUMMARY

A notch radiator was analyzed using our notch radiator analysis software. The analysis revealed that the radiator could be tuned by varying the stripline open and slotline short terminations. With only two distinct states, a low frequency state and a high frequency state, the notch radiator could be tuned to satisfy the program bandwidth, VSWR, and scan angle requirements. Stripline and slotline tuning circuitry was designed such that the notch could be electrically tuned to both the low frequency and high frequency states. The tuning circuitry (with realistic tuning device loss) was added to our notch model and the notch was reanalyzed. The predicted performance of the tuned notch is improved over the "best case" untuned notch. This Tunable Notch compensating scheme successfully satisfies the program requirements and is a viable mismatch compensation approach.

3.0 APPROACHES

3.1 Directions of Investigation

Various compensating schemes can theoretically be implemented in order to meet the system requirements. Table 3-1 lists four approaches that offer the best possibility of satisfying the system requirements.

Table 3-1
Compensating Network Approaches

1. Tunable Notch Radiator
2. Continuous Match
3. Switched Match
4. Reflective Cancelling

3.2 Tunable Notch

Figure 3-1 illustrates the Tunable Notch compensating scheme. This scheme was considered our primary approach and our efforts were concentrated on the Tunable Notch. The notch radiator input match can be changed by varying the open circuited stripline and shorted slotline termination lengths. This compensating approach minimizes the number of switching elements and therefore has the potential of low insertion loss. Also, since the tuning devices are not directly in the rf signal path, they do not see the total radiator power. This will lead to lower compensation network losses. With this scheme, the insertion loss due to the stripline and slotline compensating networks could be less than the increase in notch gain resulting from the improved input match. Therefore, the compensated notch would have improved gain over an uncompensated notch and the compensating scheme would be considered viable. With the potential of improved notch performance, the Tunable Notch

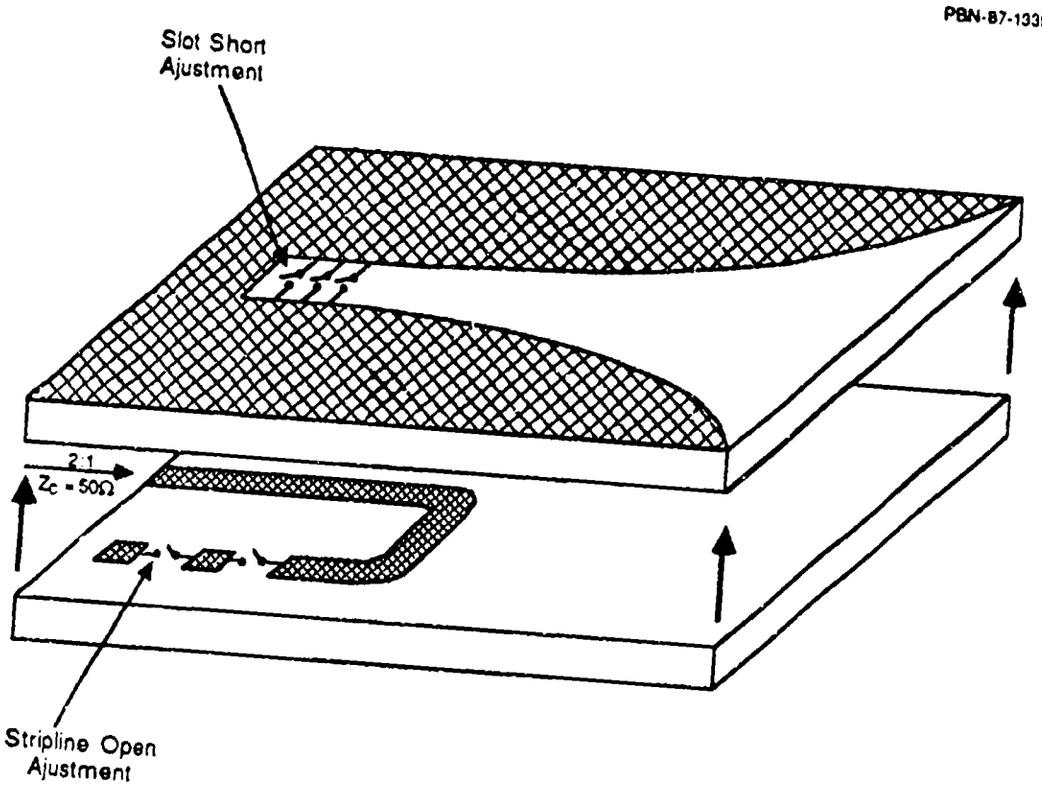

Figure 3-1. Tunable Notch Compensating Scheme.

compensating scheme was considered the most promising compensating scheme and our efforts were concentrated on this approach.

3.3 Continuous Match

The Continuous Match compensation approach is illustrated in Figure 3-2. The variable length transmission line is used to rotate the radiator impedance and then the variable reactance and susceptance are used to reduce the radiator mismatch as illustrated on the Smith chart in Figure 3-2. Many variable length transmission line sections are needed to achieve large phase shifts (full Smith chart coverage) at the low end of the frequency band. This results in a large structure which can diminish the network's instantaneous bandwidth and a large number of series varactors which will cause intolerable insertion loss. Due to these bandwidth and loss limitations, the Continuous Match approach was deemed unacceptable.

3.4 Switched Match

Figure 3-3 illustrates the Switched Match compensation approach. This is the simplest approach and is similar to the Continuous Match scheme but can offer greater instantaneous bandwidth. In the Switched Match approach, various matching structures are switched in and out in order to reduce input mismatch. Three single pole, multi-throw switches would be needed. We have built and tested MMIC single pole, multi-throw switches. Typical insertion loss of a 1 x 4 (one input, four outputs) switch ranges from 1.5 dB to 3.5 dB in the 6-18 GHz bandwidth. With three switches in the circuit, the network insertion loss would be excessive. Even with improved circuitry and devices (such as a PIN diode), a loss of 1.5 dB per switch is the very best that may be expected. Therefore, the Switched Match approach is not considered a viable compensating network.

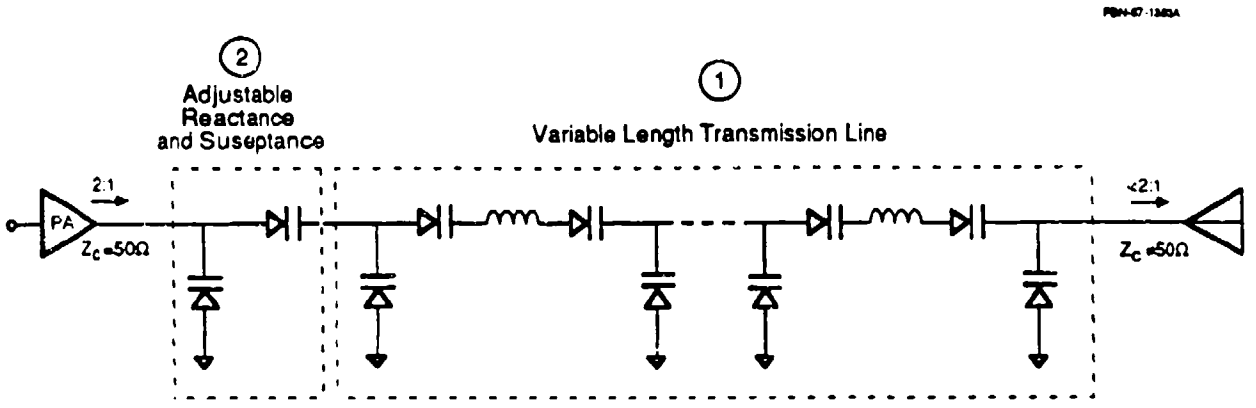

a.

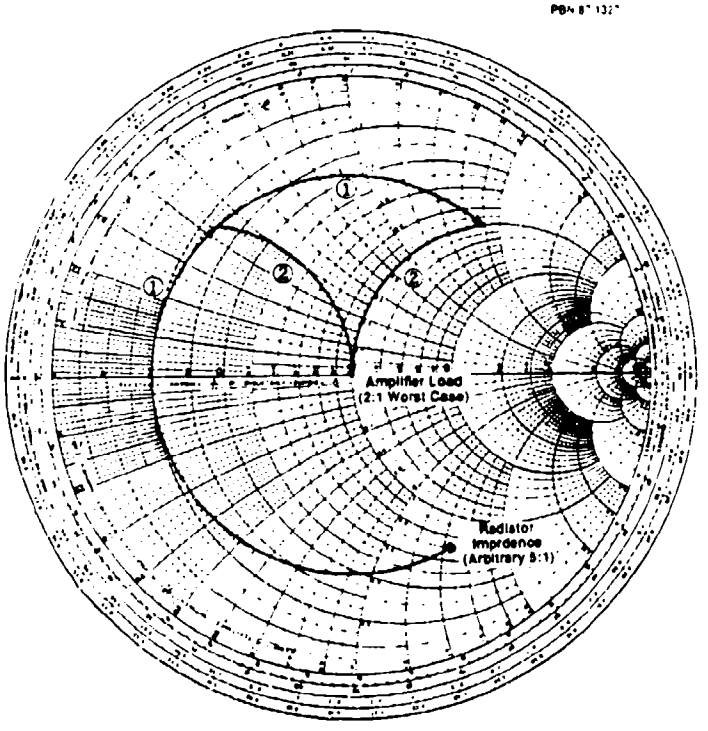

b.

Figure 3-2. Continuous Match Approach for Mismatch Compensation; a) Circuit Implementation, b) Smith Chart Representation of Operation.

PBN-87-1352

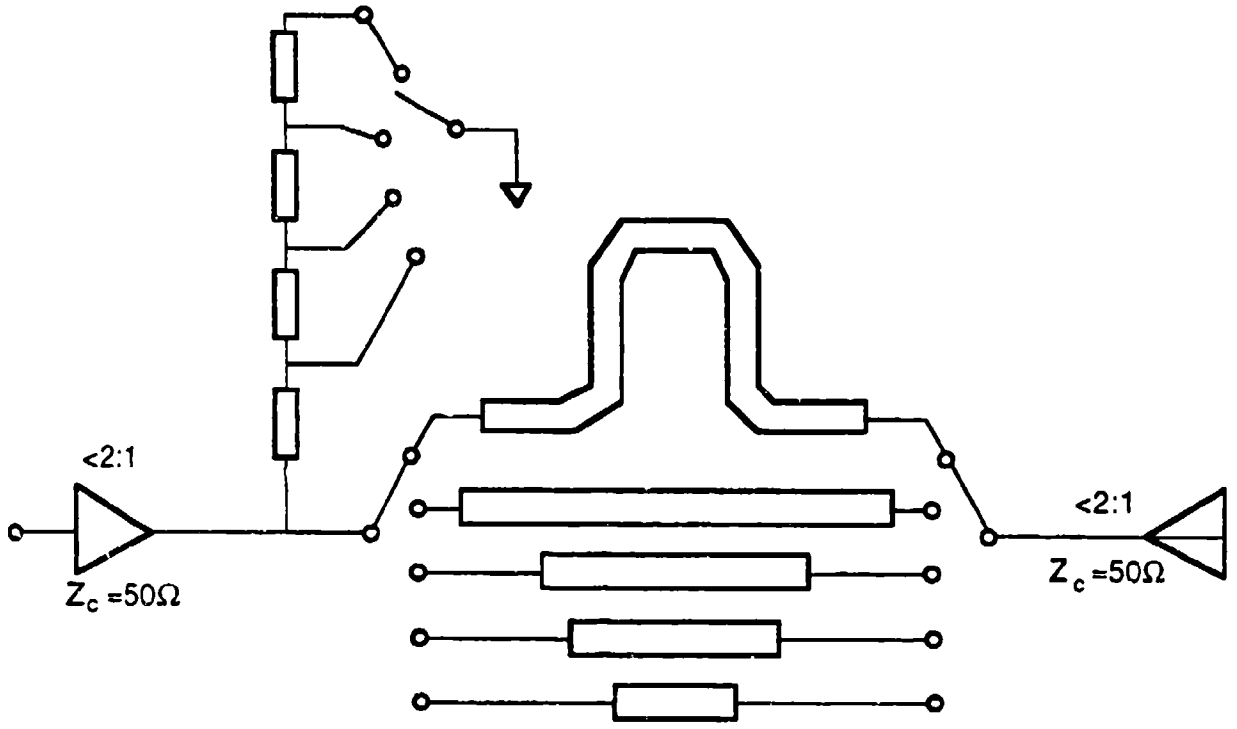

Figure 3-3. Switched Match Approach for Mismatch Compensation.

3.5 Reflective Cancelling

The Reflective Cancellation compensating scheme is illustrated in Figure 3-4. This approach uses a 90° hybrid and phase shifters to cancel reflections from the radiator. The two phase shifters are adjusted differentially to change reflection amplitude and together to change reflection phase from the hybrid. Broadband 6-18 GHz 90° hybrids have been demonstrated on MMICs by Raytheon. Typical insertion loss per pass for the hybrid is 0.5 dB, resulting in 1 dB of loss for this configuration. The phase shifters will also have considerable insertion loss. If the phase shifter loss could be held to 1 dB per pass (exceptional performance), they would still contribute an additional 2 dB of loss which would yield a total insertion loss of 3 dB. This insertion loss excludes the Reflective Cancellation scheme from being a worthy compensating approach.

PBN-88-1093

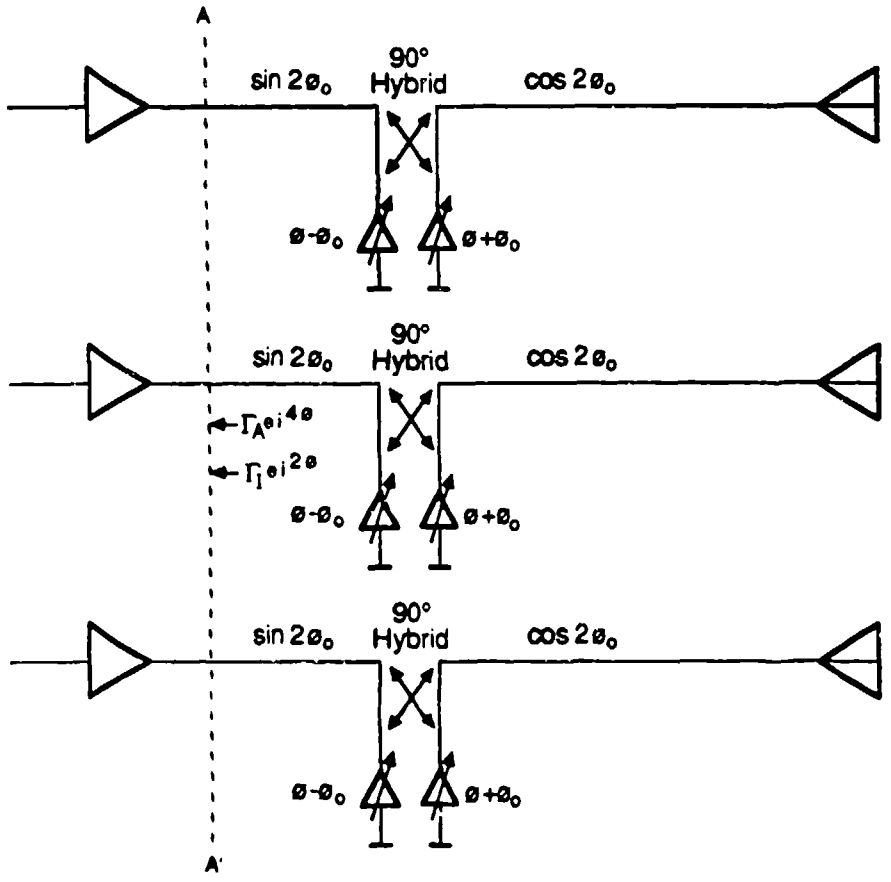

Let $\vec{\Gamma}_A$ = Array Reflection Coefficient as viewed at AA'

$\vec{\Gamma}_I$ = Reflection Coefficient that must be induced at AA' to cancel out Γ_A

Amplitude Adjustment: Vary ϕ_0 such that $\boxed{\sin 2\phi_0 = |\Gamma_A|}$

Phase Adjustment: Vary ϕ such that $2\phi = -(\angle\Gamma_A + \angle\Gamma_I)$

Figure 3-4. Reflective Cancellation Method of Mismatch Compensation.

4.0 TUNABLE NOTCH RADIATOR

4.1 Tunable Notch Compensating Scheme

The input VSWR of the notch radiator can be varied by changing the stripline and slotline termination lengths and hence reflection coefficients. The Tunable Notch compensation scheme will use this property to tune the notch such that the notch input VSWR is maintained below 2.0 from 6-18 GHz and for antenna scan angles from 0-60°.

4.2 Notch Input VSWR Dependance on the Stripline Termination Reflection Coefficient

To show the notch radiator input VSWR dependance on the stripline reflection coefficient, the stripline feed to slotline coupling region is represented as a four port network. This representation is shown in Figure 4-1. The stripline is represented by ports 1 and 2 and the slotline is represented by ports 3 and 4.

The ports are assigned to phase planes $Y = \pm a/2$ in the stripline and $X = 0^{\pm}$ in the slot. From the four port representation, we define;

$$\begin{pmatrix} V_1^- \\ V_2^- \\ V_3^- \\ V_4^- \end{pmatrix} = \begin{pmatrix} S_{11} & S_{12} & S_{13} & S_{14} \\ S_{21} & S_{22} & S_{23} & S_{24} \\ S_{31} & S_{32} & S_{33} & S_{34} \\ S_{41} & S_{42} & S_{43} & S_{44} \end{pmatrix} \begin{pmatrix} V_1^+ \\ V_2^+ \\ V_3^+ \\ V_4^+ \end{pmatrix}$$

PBN-88-747

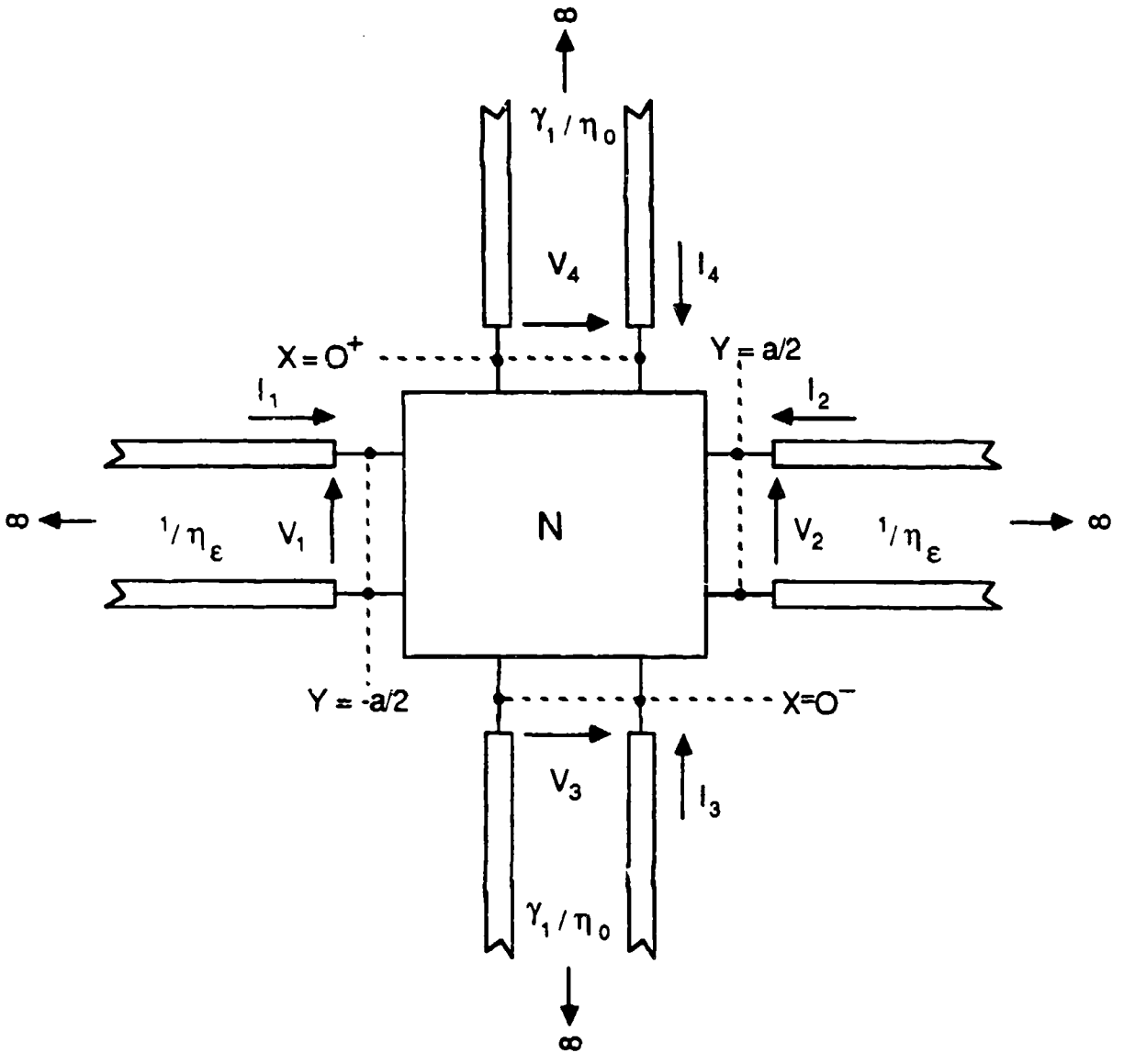

Figure 4-1. Network Representation of Infinite Slot, Infinite Stripline Coupling Region.

parameters are defined such that;

$$\text{power at port } n = V_n I_n^*$$
$$= |V_n|^2 / Z_n$$
$$= |V_n|^2 Y_n$$

where Y_n is the characteristic admittance of the line associated with port n. Requiring reciprocity and exploiting the symmetry of the structure;

$$S_{11} = S_{22} \qquad S_{23} = -S_{13} = -\bar{\eta}S_{31} \qquad S_{31} = S_{41}$$
$$S_{12} = S_{21} \qquad S_{24} = S_{23} \qquad S_{32} = -S_{31} = S_{42}$$
$$S_{13} = \bar{\eta}S_{31} \qquad S_{33} = S_{44}$$
$$S_{14} = S_{13} = \bar{\eta}S_{31} \qquad S_{34} = S_{43}$$

where η is the ratio of surface wave admittance, $Y_s = k_x/k\eta o$, to stripline wave admittance and the negative sign preceding certain scattering parameters is due to the reversal of direction of the slot field via excitation of port 1 compared with that of port 2 (the stripline ports). The scattering matrix can now be expressed as;

$$S = \begin{pmatrix} S_{11} & S_{21} & \bar{\eta}S_{31} & \bar{\eta}S_{31} \\ S_{21} & S_{11} & -\bar{\eta}S_{31} & -\bar{\eta}S_{31} \\ S_{31} & -S_{31} & S_{33} & S_{43} \\ S_{31} & -S_{31} & S_{43} & S_{33} \end{pmatrix}$$

After applying lossless conditions to the scattering matrix, the input reflection coefficient (Γ_{in}) can be expressed as;

$$\Gamma_{in} = \frac{\frac{S_{11}}{\alpha} - 2S_{11} + \frac{C}{\alpha} - 2C + 1}{\frac{1}{\alpha} - S_{11} - C}$$

where C is not a function of α and α is the reflection coefficient of the open circuit terminated stripline (V_2^+/V_2^-) at Y = a/2 (see Appendix A). The notch radiator input match can therefore be varied by changing the stripline reflection coefficient. The stripline reflection coefficient can be varied by adding tuning circuitry to the stripline such that its electrical length can be changed.

4.3 Notch Radiator Analysis Software

A numerical approximation for lossless, arrayed notch radiator active reflection coefficients was developed under Air Force contract F19628-72-C-0202 [1]. This code has successfully provided starting points for the empirical design of array radiators, and for narrow band radiators, has successfully predicted element patterns in both E- and H-planes. For the present program, the analysis code has been employed to arrive at baseline notch geometries and tuning circuit characteristics.

The basic analytical technique employed in the computer program is to develop approximate modal expansions for the fields in each uniform region of the array structure, and in the vicinity of each array cell discontinuity, then perform a Galerkin procedure to match fields at all discontinuities, assuming single mode content in the immediate vicinity of the slotline/stripline junction. As a result of single mode field matching across the slotline interface, an approximate description of stripline to slotline scattering is obtained. The field equations are then reduced to a transmission line

scattering formulation with the physical junction region represented by a four port scattering matrix, as illustrated previously in Figure 4-1. Ports 2 and 3 terminate in an open circuit and short circuit respectively. Port 4 is connected via a non-uniform transmission line representing slitted parallel plate propagation to the radiating aperture. Since the characteristics of all terminations are known, solution of the resulting scattering matrix results in an estimate of radiator reflection coefficient.

4.4 Nominal Notch Design

A notch radiator was designed using the notch radiator analysis software. The radiator was designed for minimum VSWR in an array environment from 6-18 GHz and antenna scan angles from 0-60°. Figure 4-2 shows the notch radiator dimensions. The element to element spacing in the array is 0.268" in both the X and Y directions. Figure 4-3 shows the notch input VSWR vs. frequency for various scan angles up to 64.16° for this nominal notch design. The notch input VSWR is roughly symmetric (i.e., similar VSWR at the frequency band edges) in the frequency band. Maximum notch input VSWR is 3.8:1 and occurs at both the low and high frequency band edges. Using this notch design as the nominal design, we tuned the notch to meet the system requirements by varying the stripline and slotline termination lengths. All the other nominal notch dimensions and array spacing remained fixed throughout the remainder of the program.

4.5 Low Frequency Tuned Notch

The nominal notch was tuned by varying the stripline termination length (using the notch radiator analysis software) in order to reduce the input VSWR at the low end of the frequency band. The input VSWR could not be reduced below 2.0 at the low end of the frequency band by changing the stripline length only. After varying the slotline termination length, it became apparent

PBN-88-0042

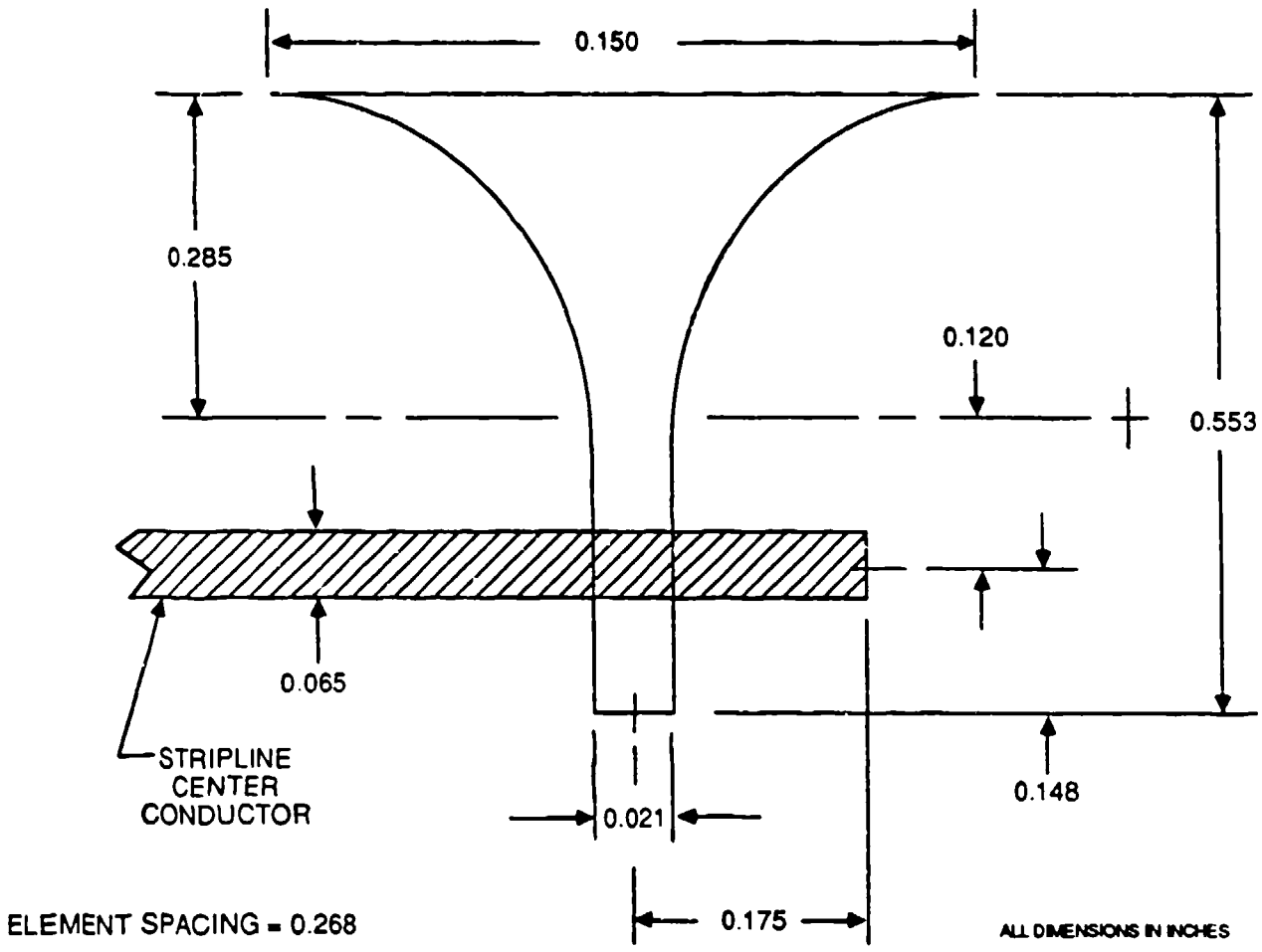

Figure 4-2. Nominal Notch Radiator Dimensions.

PBN-88-0043

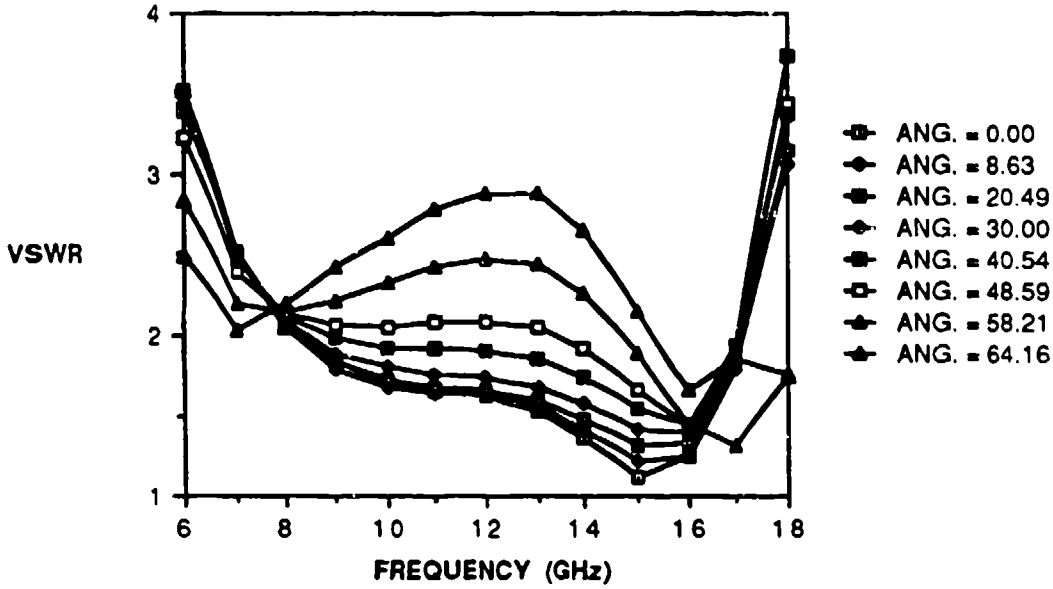

Figure 4-3. Nominal Notch Input VSWR vs.Frequency.

that the slotline termination controls the low frequency cutoff of the notch radiator. Therefore, to reduce the notch input VSWR at the low frequencies, the slotline termination length was increased from 0.148" in the nominal design to 0.220". Further tuning was performed by increasing the stripline termination length from 0.175" to 0.185". With these stripline and slotline termination lengths, the nominal notch was tuned to a low frequency design such that the notch input VSWR was less than 2.0 (input reflection coefficient less than 0.333) at the low end of the frequency bandwidth. Figure 4-4 shows input reflection coefficient contours vs. frequency and Sine of the scan angle for the low frequency notch design. The input reflection coefficient of the low frequency design is less than 0.333 for frequencies from 6-15 GHz and antenna scan angles from 0-60° (sin(60°) = 0.866). The sensitivity of the low frequency design was investigated by varying the stripline and slotline terminations +/- 0.005" from their optimum low frequency design lengths. With the stripline termination at its optimum length of 0.185", Figure 4-5 shows the notch input reflection contours when the slotline termination length is 0.215" (0.005" shorter than optimum) and Figure 4-6 shows the notch input reflection coefficient contours when the slotline termination length is 0.225". With the slotline termination at its optimum length of 0.220", Figure 4-7 shows the notch input reflection coefficient contours with a stripline termination length of 0.180" (0.005" shorter than optimum) and Figure 4-8 shows the notch input reflection coefficient contours with a stripline termination length of 0.190". There is little change in the notch input reflection coefficient from 6-15 GHz when either the stripline or slotline terminations are varied by 0.005" from their optimum low frequency design lengths. This indicates a notch design that is stable and producible within typical manufacturing tolerances. With only one tuned notch state, the system input VSWR and scan angle requirements are satisfied from 6-15 GHz.

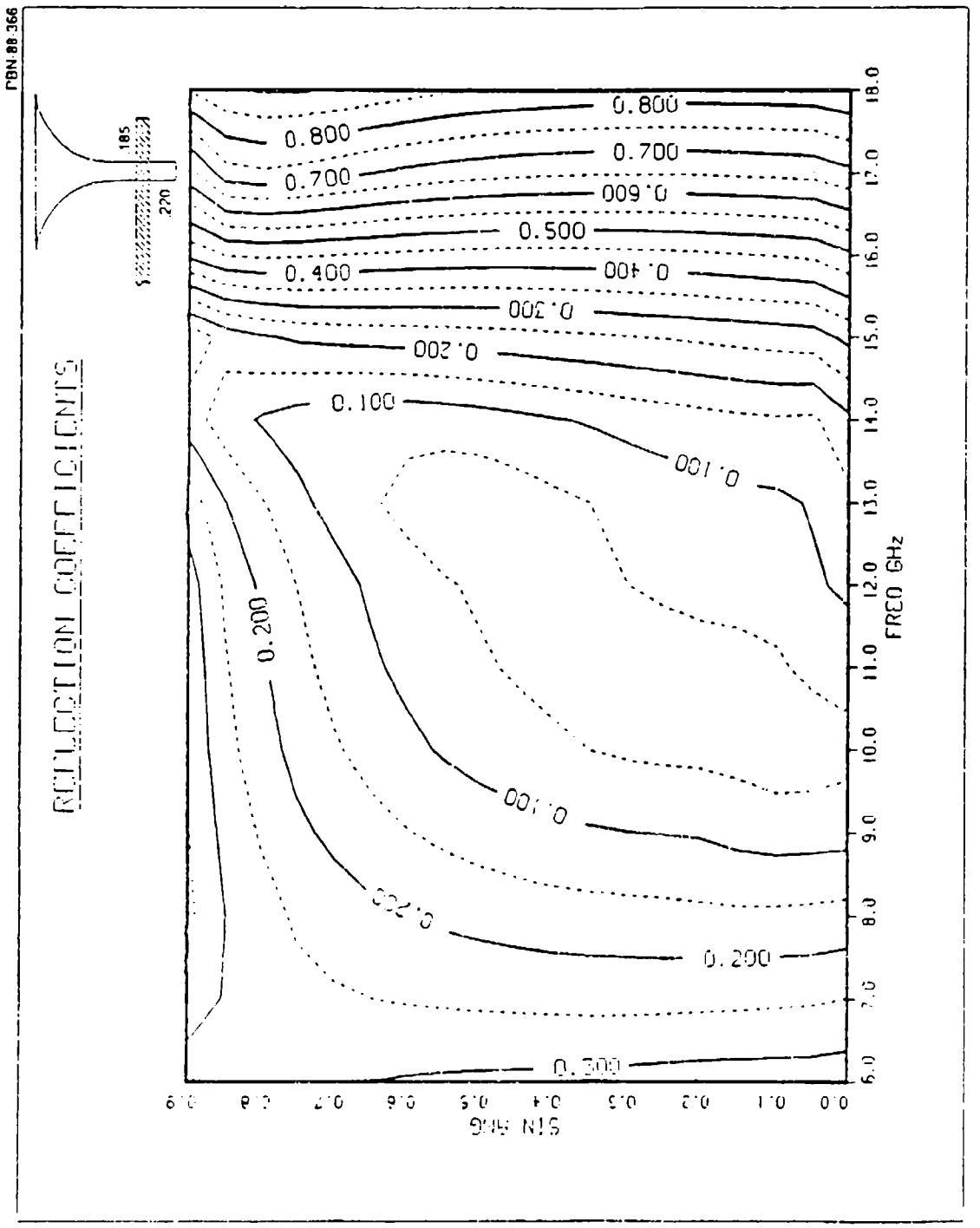

Figure 4-4. Low Frequency Notch Design Input Reflection Coefficient Contours.

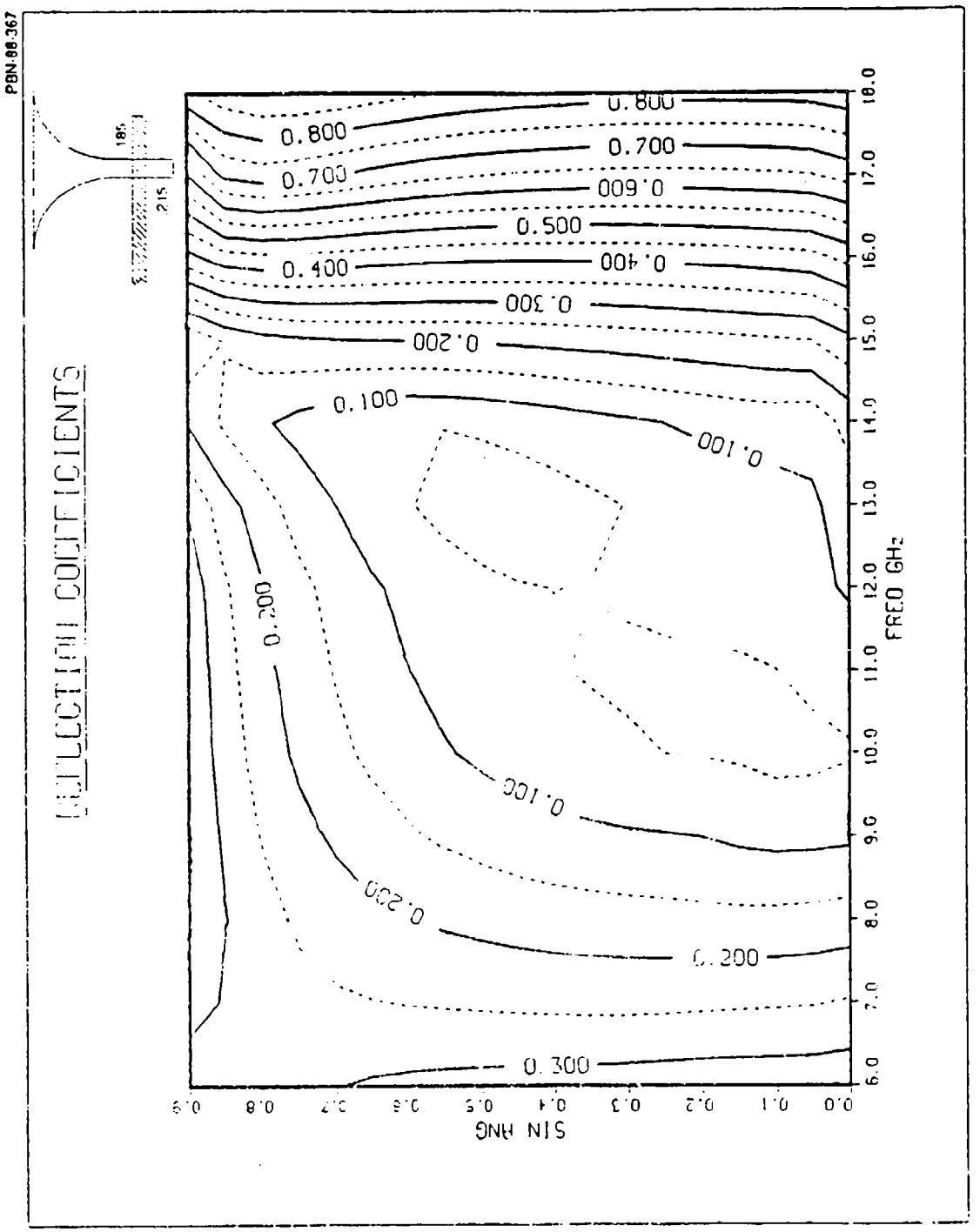

Figure 4-5. Input Reflection Coefficient Contours of the Notch with the Slotline 0.005" Shorter than the Low Frequency Design.

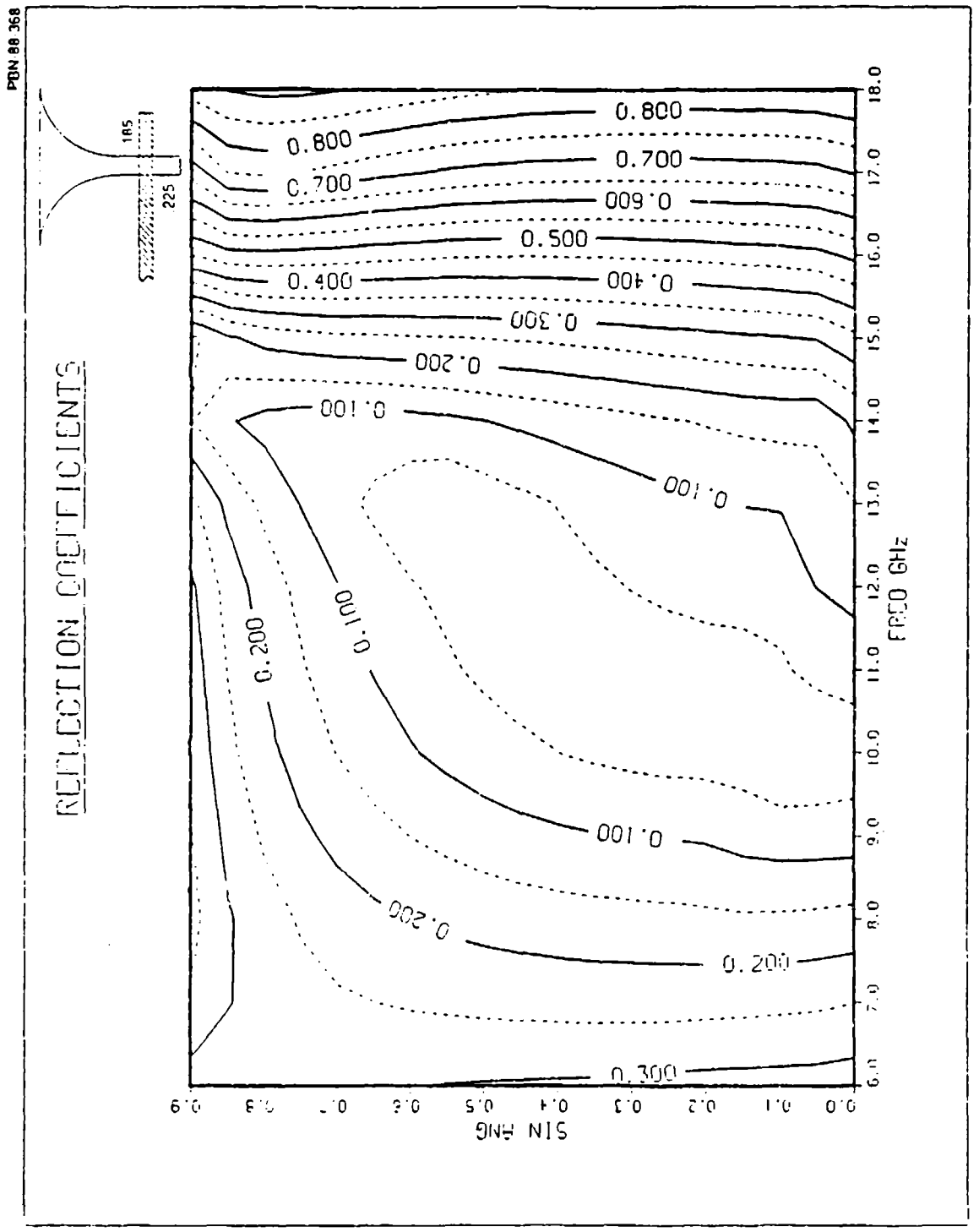

Figure 4-6. Input Reflection Coefficient Contours of the Notch with the Slotline 0.005" Longer than the Low Frequency Design.

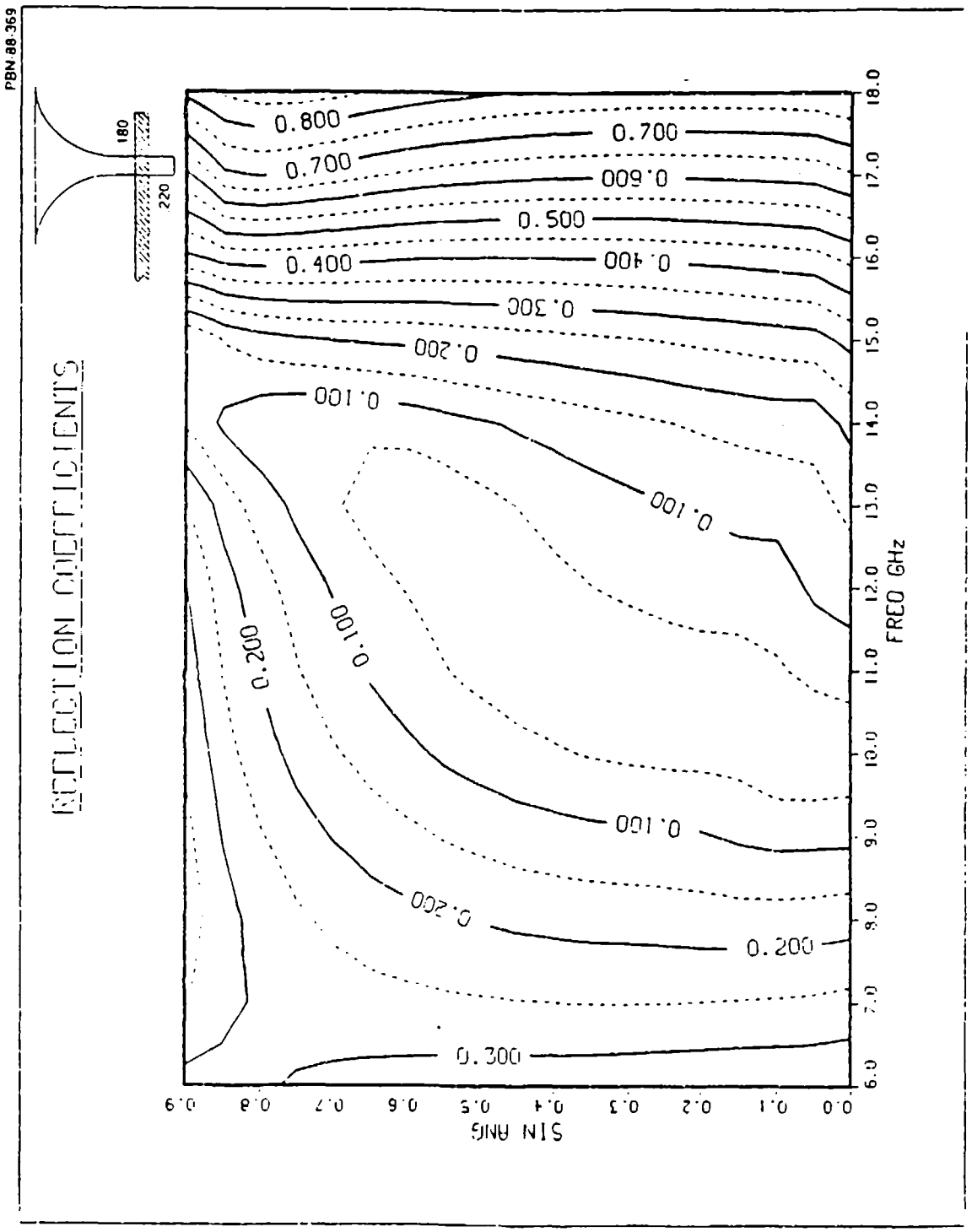

Figure 4-7. Input Reflection Coefficient Contours of the Notch with the Stripline 0.005" Shorter than the Low Frequency Design.

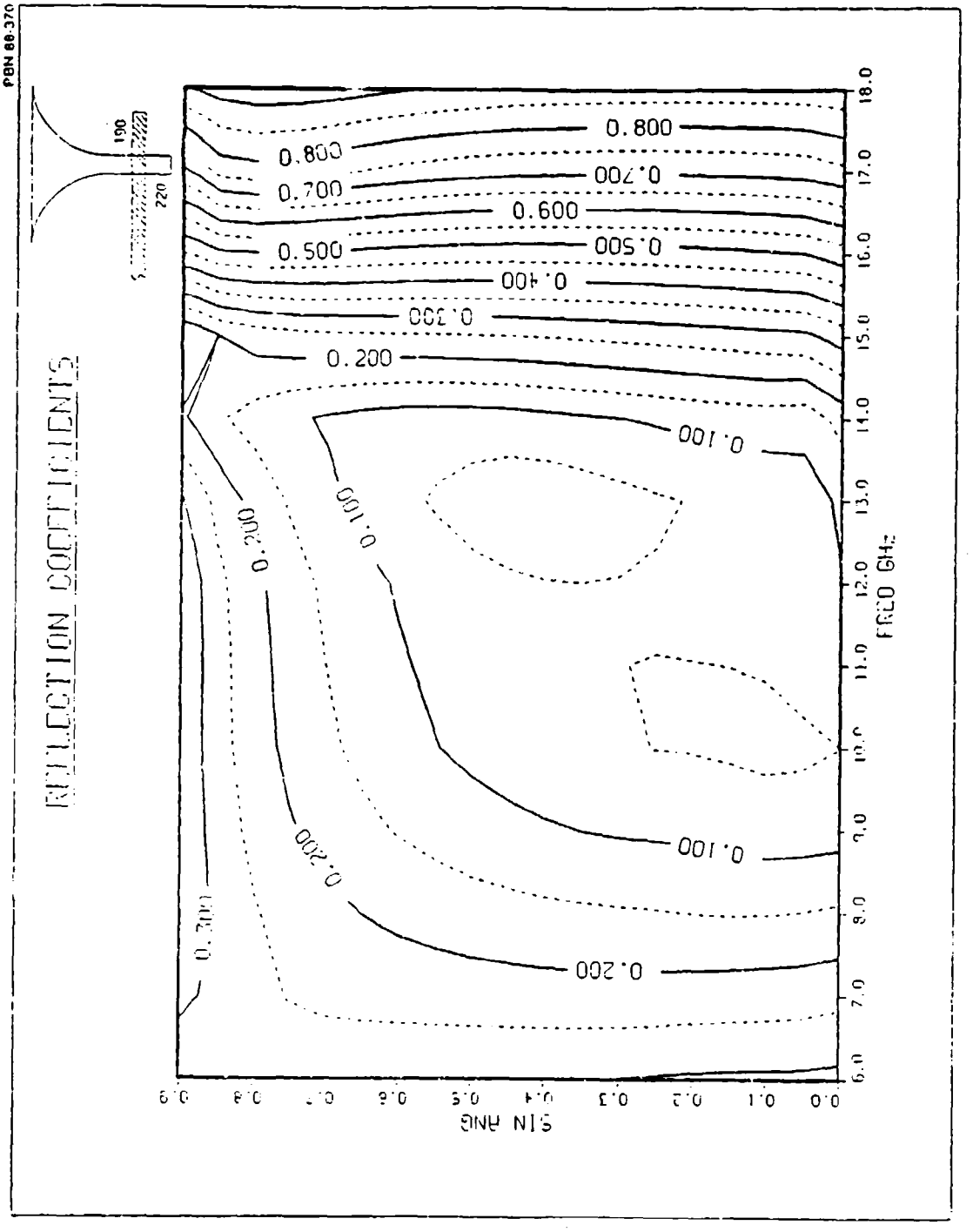

Figure 4-8. Input Reflection Coefficient Contours of the Notch with the Stripline 0.005" Longer than the Low Frequency Design.

4.6 High Frequency Tuned Notch

The nominal notch was then tuned to reduce the input VSWR at the high end of the frequency band. Since the slotline termination length controls the low frequency cutoff of the notch, the slotline termination length had to be decreased to reduce the notch input VSWR at the high end of the frequency band. Further notch tuning was performed by reducing the stripline termination length. Figure 4-9 shows the notch input reflection coefficient contours vs. frequency and Sine of the scan angle when the slotline termination length is 0.125" and the stripline termination length is 0.160". The notch input reflection coefficient is less than 0.333 for frequencies from 14.5 to 18 GHz and scan angles up to 60°. The high frequency design sensitivity was investigated by varying the stripline and slotline terminations +/- 0.005" from their optimum high frequency design lengths. With the stripline termination length equal to 0.160", Figure 4-10 shows the notch input reflection coefficient contours when the slotline termination length is 0.120" (0.005" shorter than its optimum length) and Figure 4-11 shows the notch input reflection coefficient contours when the slotline termination length is 0.130". With the slotline termination length equal to 0.125", Figure 4-12 shows the notch input reflection coefficient contours when the stripline termination length is 0.155" (0.005" shorter than its optimum length) and Figure 4-13 shows the notch input reflection coefficient contours when the stripline termination length is 0.165". With the slotline termination length equal to 0.120" (0.005" shorter than optimum), the notch input reflection coefficient is greater than 0.333 at 15 GHz for high scan angles. With the stripline termination length equal to 0.165" (0.005" longer than optimum), the notch input reflection coefficient exceeds 0.333 at the high frequency band edge for scan scan angles around 35°. For the majority of the 15-18 GHz bandwidth and scan angles from 0-60°, the notch input VSWR remains less

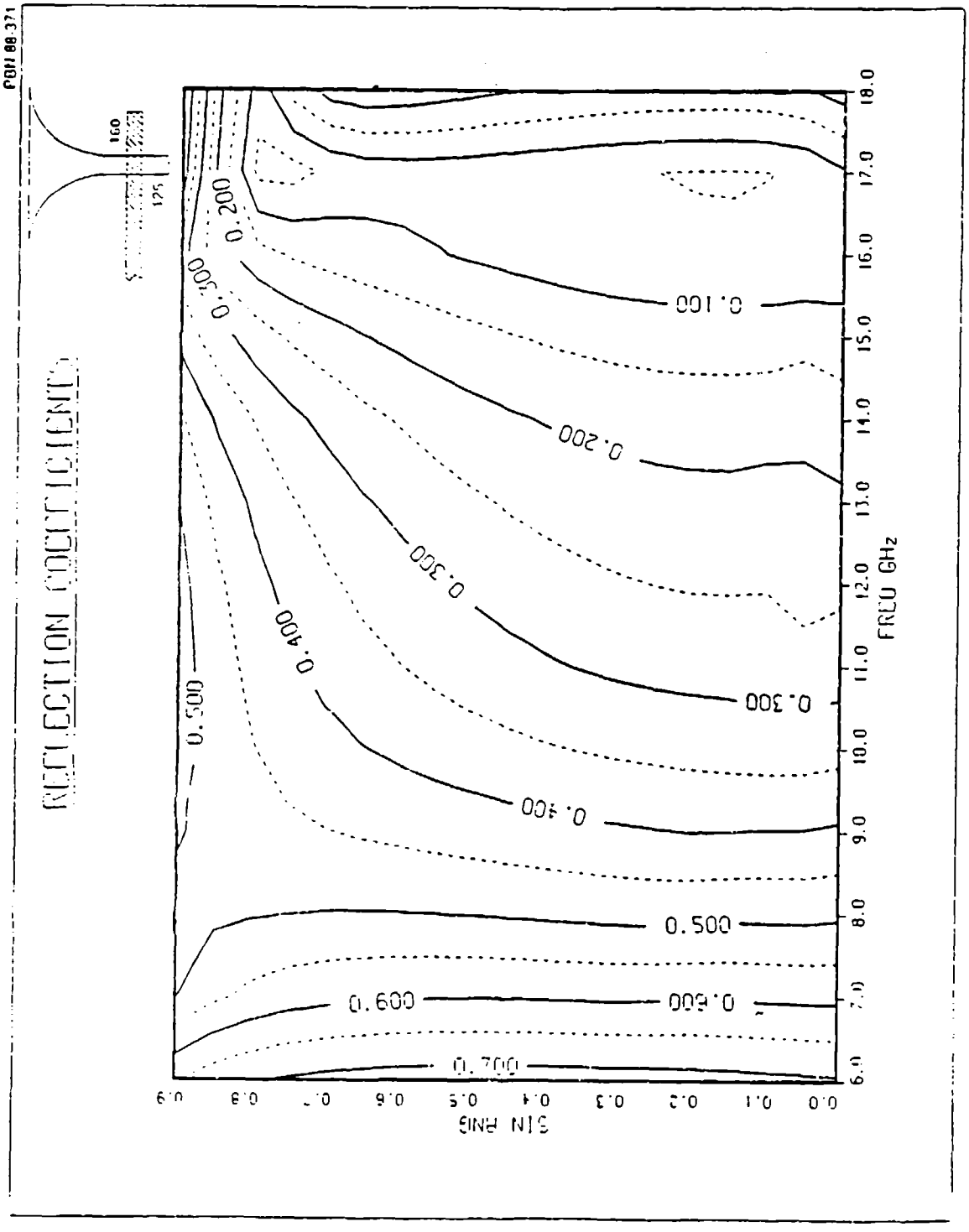

Figure 4-9. High Frequency Notch Design Input Reflection Coefficient Contours.

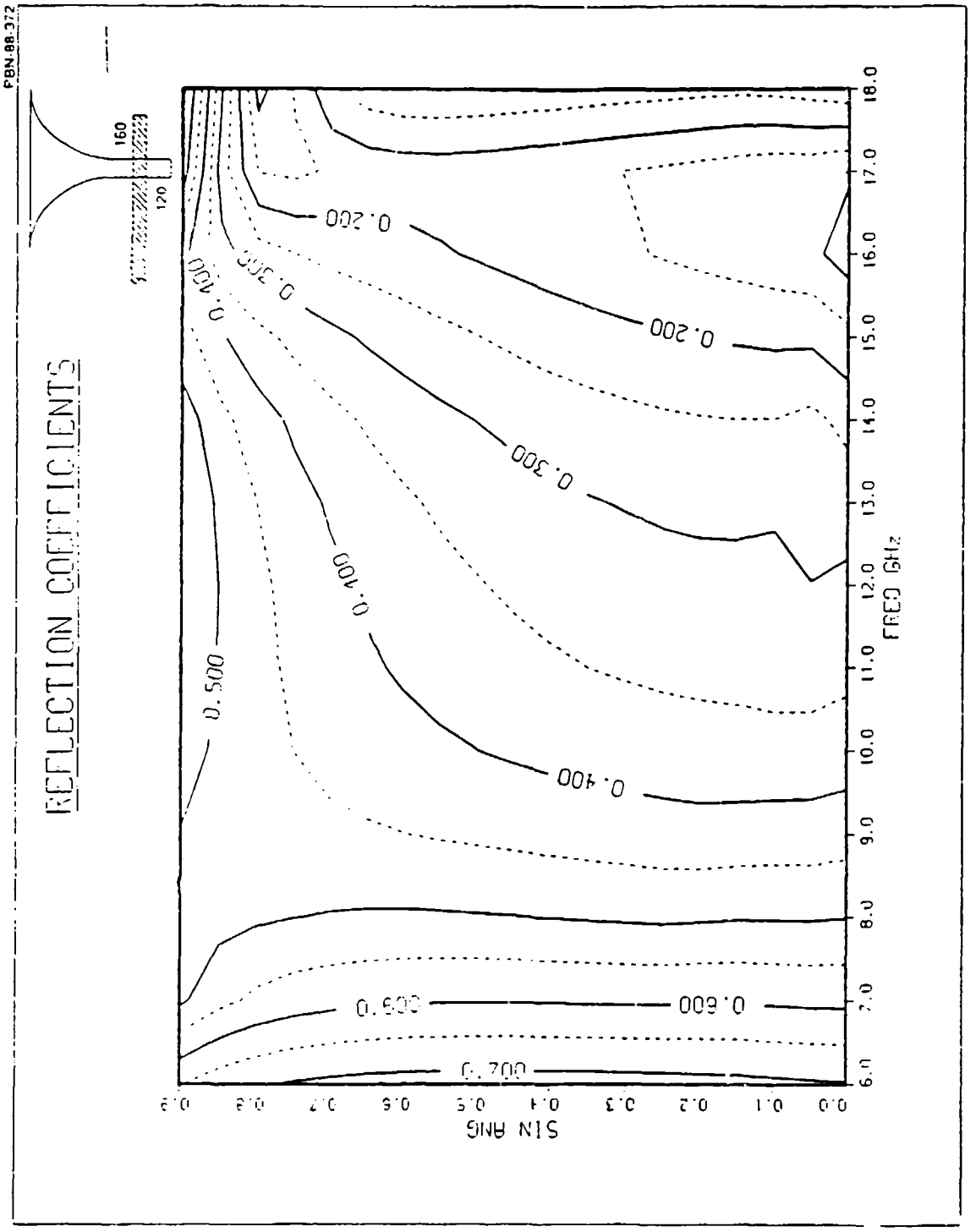

Figure 4-10. Input Reflection Coefficient Contours of the Notch with the Slotline 0.005" Shorter than the High Frequency Design.

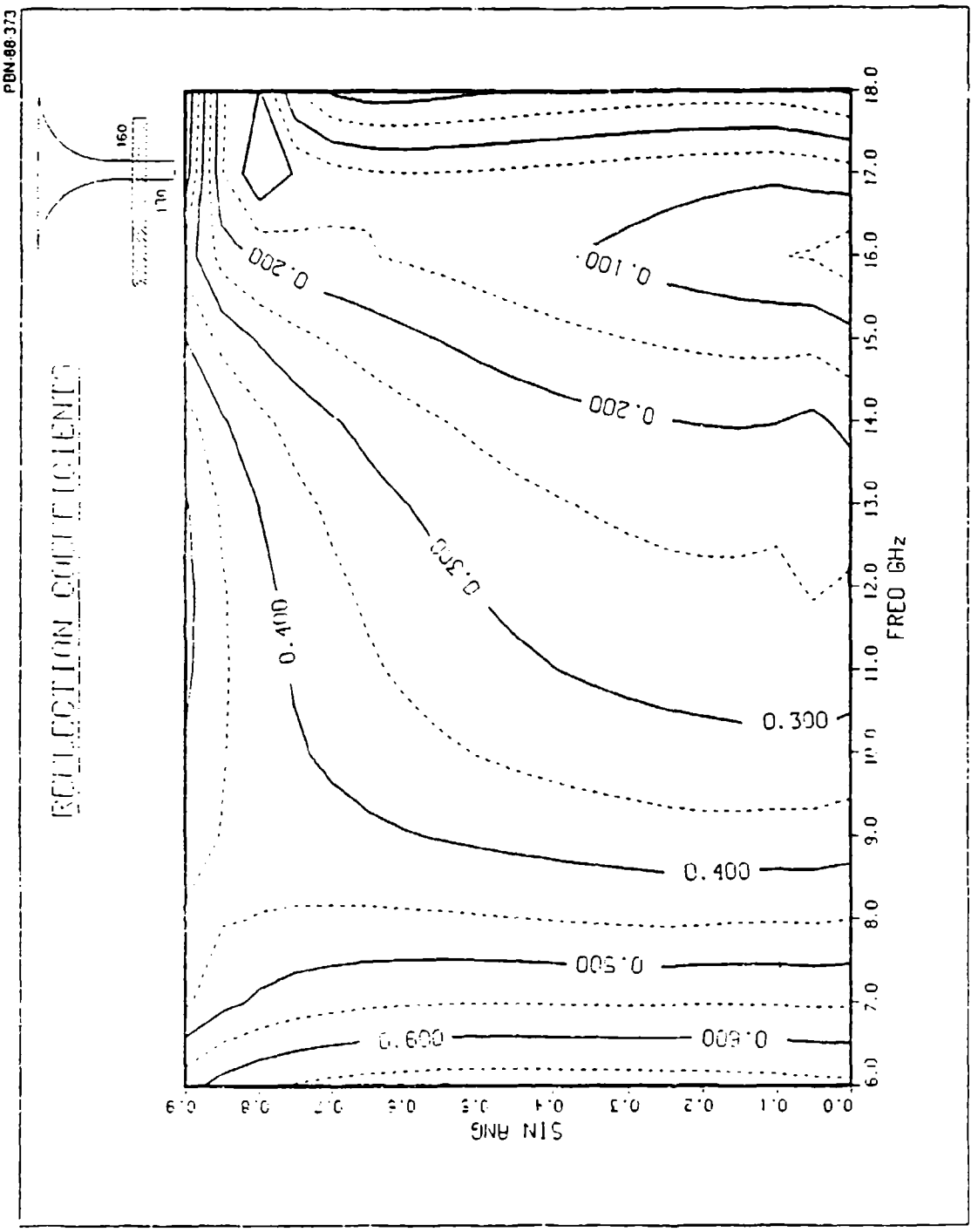

Figure 4-11. Input Reflection Coefficient Contours of the Notch with the Slotline 0.005" Longer than the High Frequency Design.

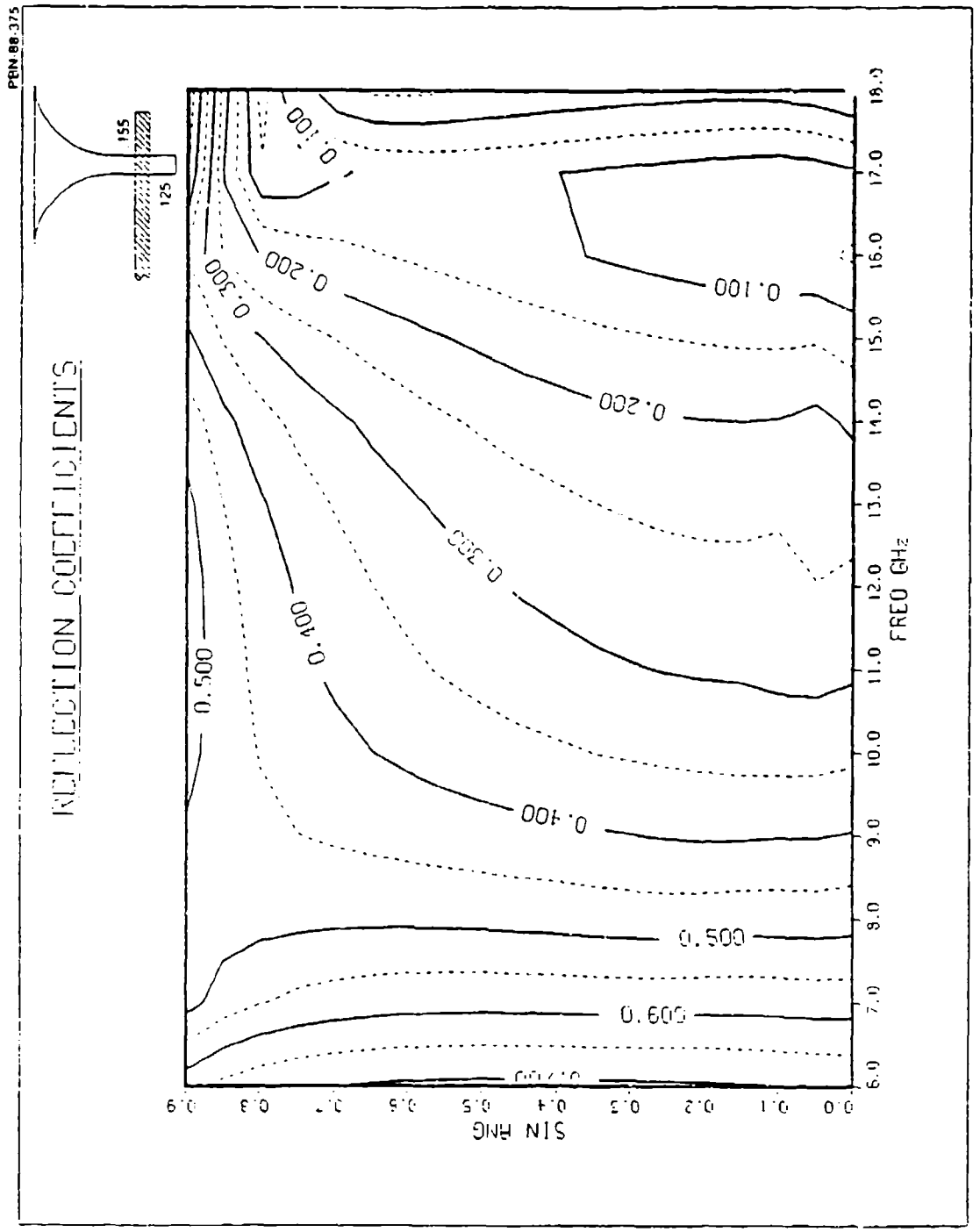

Figure 4-12. Input Reflection Coefficient Contours of the Notch with the Stripline 0.005" Shorter than the High Frequency Design.

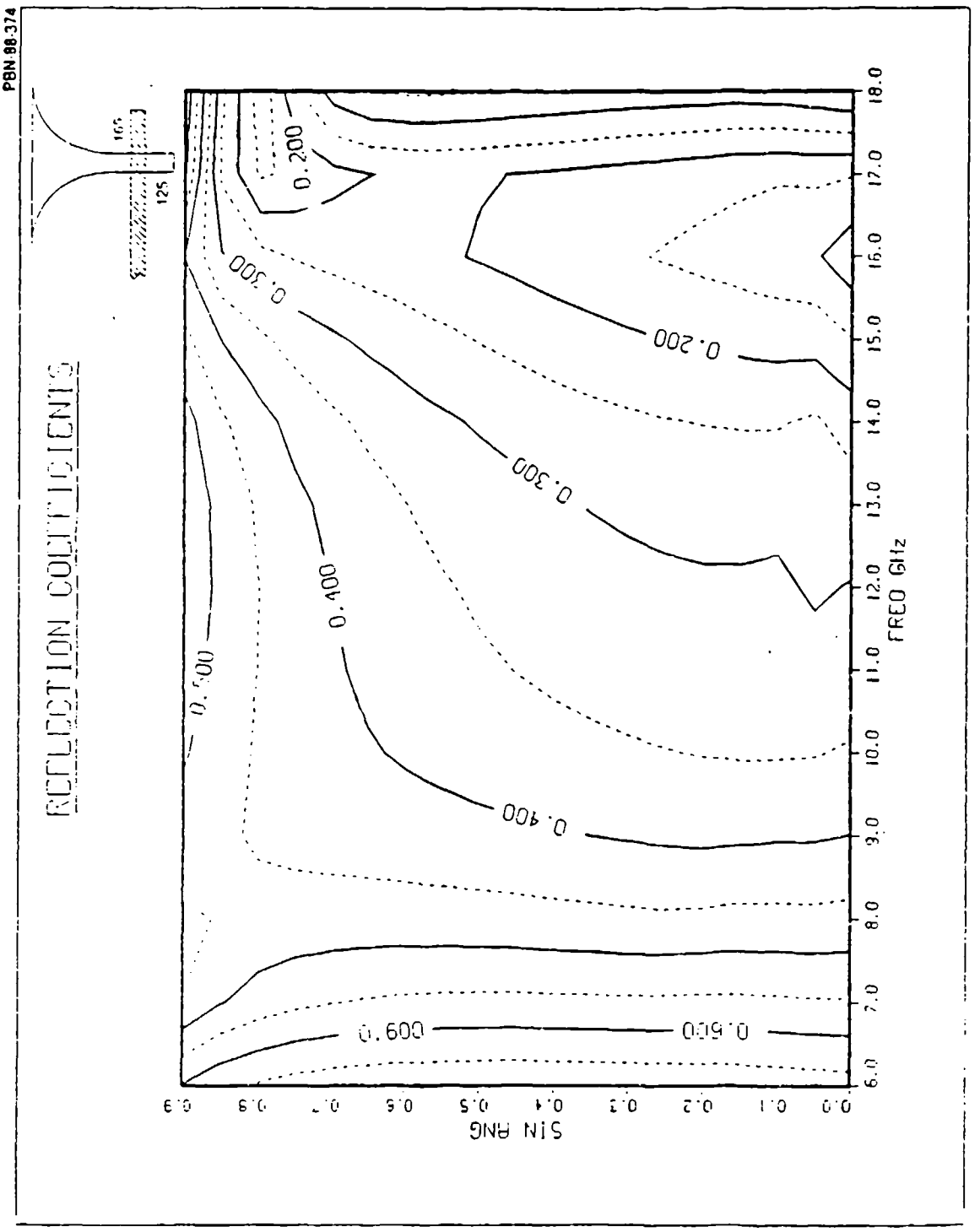

Figure 4-13 Input Reflection Coefficient Contours of the Notch with the Stripline 0.005" Longer than the High Frequency Design.

than 2.0 with 0.005" variations in the stripline and slotline terminations from their optimum high frequency design lengths.

4.7 Dual-State Notch

With only two distinct states, a low frequency state and a high frequency state, the notch radiator can be tuned to meet all the system bandwidth, VSWR, and scan angle requirements. By adding stripline and slotline tuning circuitry, a single notch can be designed that will meet the system requirements. Figure 4-14 illustrates the low frequency, high frequency, and dual-state notch designs. For the dual state notch, the stripline tuning circuitry must be able to produce the required stripline reflection coefficients associated with the low frequency termination length of 0.185" and the high frequency termination length of 0.160". The slotline tuning circuitry must be able to change the slotline termination length from 0.220" in the low frequency design to 0.125" in the high frequency design.

4.8 Stripline Termination Tuning Circuitry

The low and high frequency stripline termination reflection coefficients were determined using the notch radiator analysis software. A tuning circuit was designed and modelled that produced the required low and high frequency state stripline reflection coefficients. The tuning circuit consists of a length of transmission line and a variable capacitance to ground. The variable capacitance can change the stripline electrical length such that both the low and high frequency state reflection coefficients can be obtained. With a common transmission line length of 0.075" (width still equal to 0.065"), both the low and high frequency state reflection coefficients can be obtained when the variable capacitor is changed from 0.82pF to 0.30pF. This swing in capacitance, less than 3:1, can be easily obtained from present tuning devices.

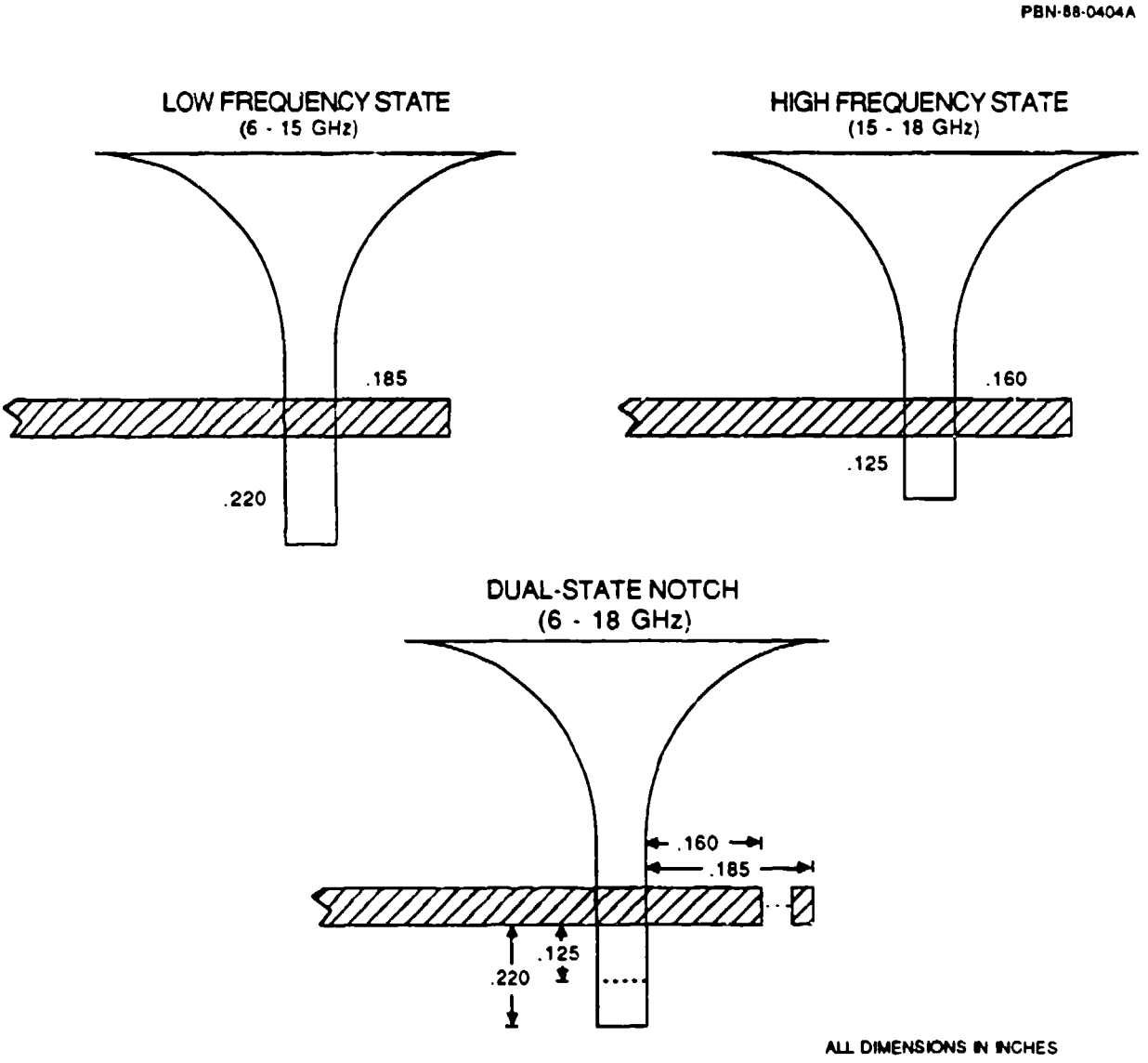

Figure 4-14 Low Frequency, High Frequency, and Dual-State Notch Designs.

Varactors can be used as the variable capacitance element in the stripline tuning circuit. A varactor can be modelled as a series resistor and capacitor. The series resistance is the source of varactor loss. Varactors can have low series rf resistance and therefore tuning circuits utilizing varactors can have low loss. Varactors with the needed capacitance range were measured at X-band frequencies (through small signal measurements) in order to determine their series resistance. Figure 4-15 shows the low and high frequency open circuited stripline states and the low and high frequency tuning circuit states with the complete lossy varactor model. The stripline tuning circuit was added to the notch analysis software and the notch was reanalyzed. The slotline was still represented by its ideal lossless low or high frequency state reflection coefficients.

4.9 Notch Input VSWR with the Stripline Tuning Circuit

Figure 4-16 shows the notch input VSWR vs. frequency for the nominal, low frequency state, and high frequency state tuned notch at 0°, 30°, and 64° scan angles. The notch input VSWR is less than 2.0 from 6-15 GHz for the low frequency design and less than 2.0 from 15-18 GHz for the high frequency design for scan angles up to 60°. Although the input VSWR goes above 2.0 for the high frequency design at 18 GHz at a scan angle equal to 64°, interpolating the VSWR data at 58° ($\sin^{-1}(0.85)$) and 64° ($\sin^{-1}(0.90)$) gives a VSWR less than 2.0 for the high frequency design at 18 GHz and a scan angle equal to 60°. These results show that the stripline tuning circuit adequately produces the required low and high frequency state stripline reflection coefficients. With these two tuned states, the notch input VSWR is less than 2.0 from 6-18 GHz and antenna scan angles from 0-60°.

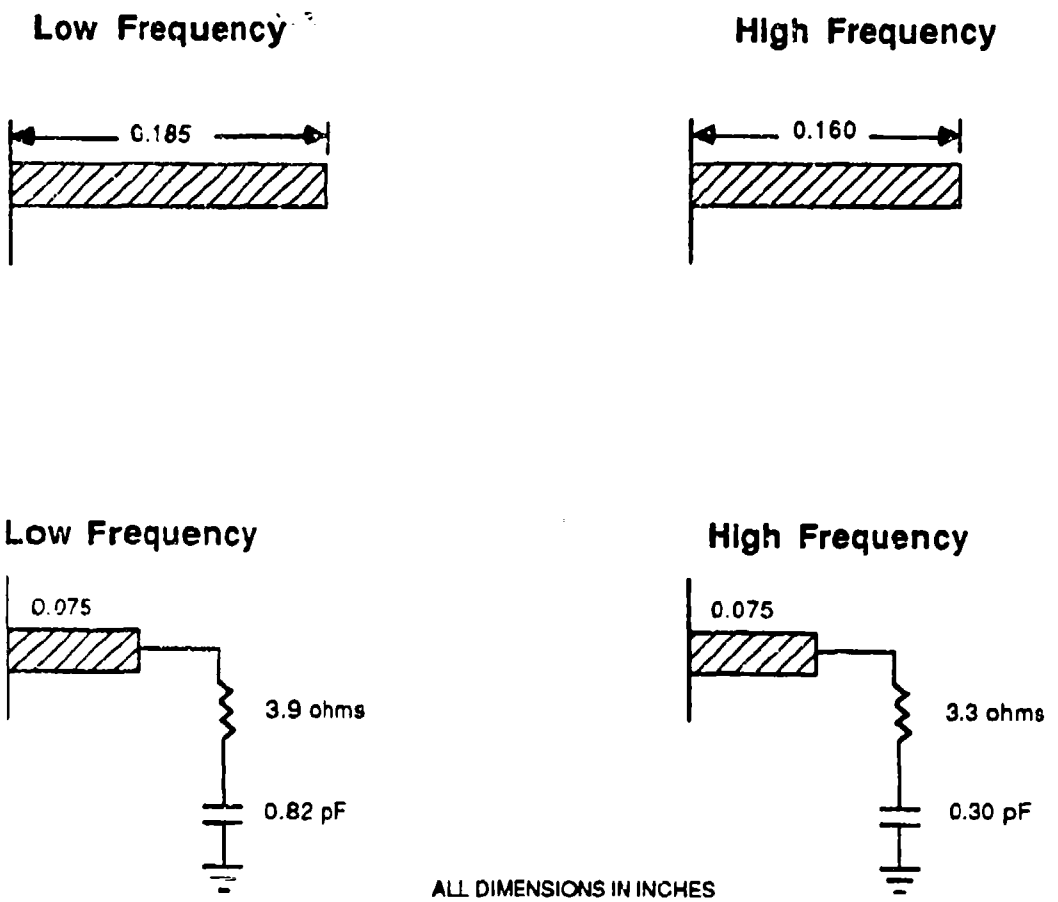

Figure 4-15. Open-Circuited Stripline and Stripline Tuning Circuit States.

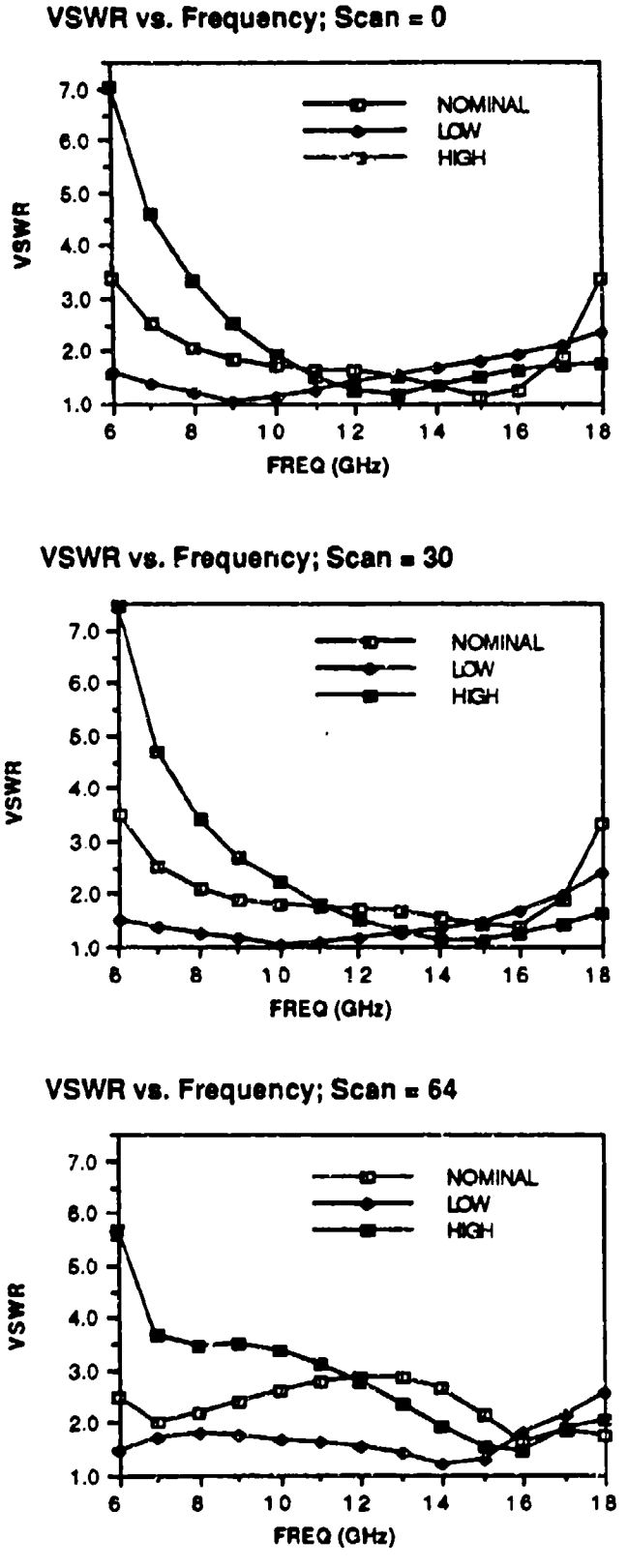

Figure 4-16. Notch Input VSWR vs. Frequency.

4.10 Notch Power Gain with the Stripline Tuning Circuit

Figure 4-17 shows the notch power gain for the nominal, low frequency state, and high frequency state tuned notch at 0°, 30°, and 64° scan angles. The low and high frequency tuned notch includes the lossy stripline tuning circuit. In all cases, the slotline is still represented by lossless reflection coefficients. In all the notch analysis, the nominal notch is assumed to be totally comprised of lossless elements. Any loss in notch power gain for the nominal notch is strictly due to input mismatch loss. For the low and high frequency tuned notch, the loss in notch power gain is due to mismatch loss and dissipation loss caused by the lossy stripline tuning circuit. The tuned notch has higher power gain than the nominal notch at the frequency band edges. This is due to the nominal design having a large VSWR and hence mismatch loss at the frequency band edges. In the middle of the frequency band, the nominal notch in general has a low VSWR (see Figure 4-16) and therefore its power gain is high at these frequencies. Even though the low and high frequency tuned notch combines for a low VSWR across the entire frequency band, the power gain of the low and high frequency tuned notch is degraded by the lossy stripline tuning circuit.

4.11 Amplifier Load Pull

A more realistic assessment of the notch power gain includes load pull affects on the radiator power amplifier. A power amplifier is designed for operation into a specific output impedance (typically 50 Ω). If the amplifier operates into an impedance other than its designed impedance, its performance will not be optimal. In a T/R module, the radiating element represents the power amplifier's output impedance. In the case of the notch radiator, at points of high input VSWR (impedance not near 50 Ω), the notch will not present an optimal load impedance to the power amplifier and performance degradation can occur.

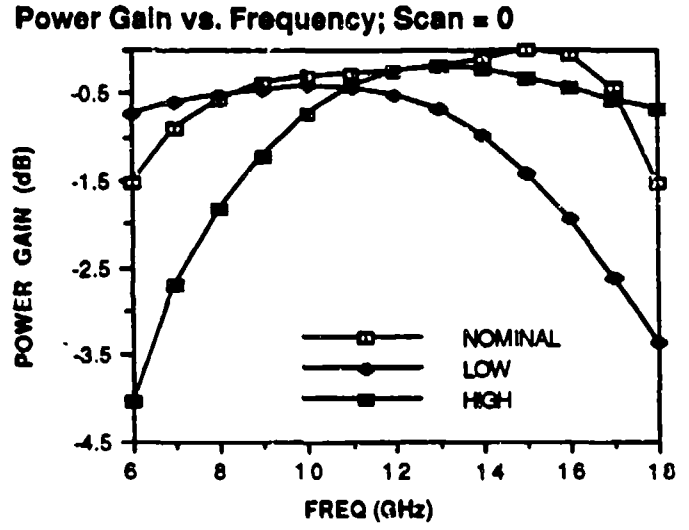

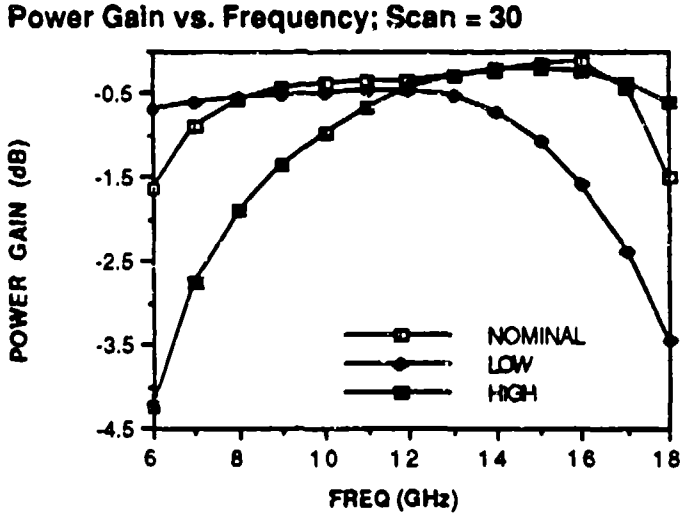

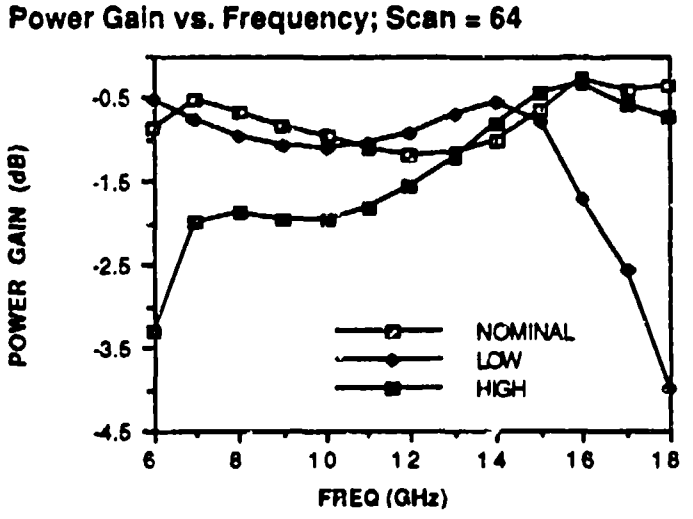

Figure 4-17. Notch Power Gain vs. Frequency.

Load pull measurements were performed at a frequency of 10 GHz on a Raytheon, wideband, balanced power amplifier. A block diagram of the amplifier is shown in Figure 4-18 and the load pull set-up is illustrated in Figure 4-19. The gain of the amplifier was measured with various load impedances. Figure 4-20 shows the load pull results plotted on a Smith chart with the amplifier's maximum power point transformed to the center of the Smith chart (same transformation applied to all data points). At an input VSWR of 2:1, the amplifier's performance was degraded by less than 0.3 dB. At a VSWR of 3:1, there is less than 0.5 dB gain degradation.

4.12 Notch Power Gain with the Stripline Tuning Circuit and Load Pull Affects

The load pull results were coupled with the prior notch VSWR and power gain data. Although load pull measurements were performed only at 10 GHz, it was assumed that the amplifier's performance similarly degraded throughout the 6-18 GHz frequency band. Figure 4-21 shows the normalized system power gain (actual amplifier gain not included, just degradation from optimum performance) for the nominal, low frequency, and high frequency notch for scan angles of 0°, 30°, and 64°. At frequencies of low notch input VSWR, there is little gain degradation. At the frequency band edges, where the nominal notch has high input VSWR, the system power gain with the nominal notch is severely degraded. With the low frequency tuned notch, from 6-15 GHz the notch input VSWR is low and therefore there is little system gain degradation. Similarly, for the high frequency tuned notch, from 15-18 GHz the notch input VSWR is low and there is little system gain degradation. At the frequency band edges, there is as much as 2 dB less loss with the tuned notch than with the nominal notch.

PBN-88-1092i

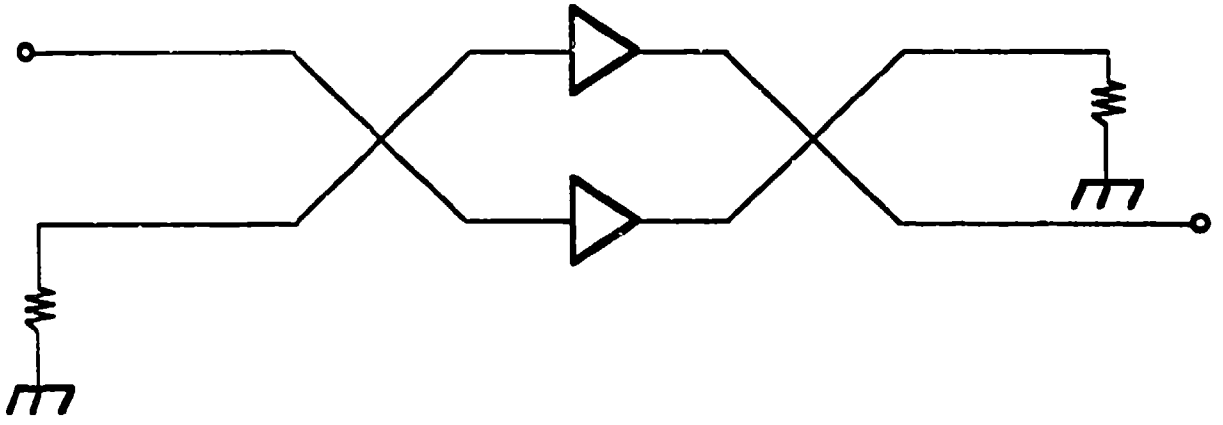

Figure 4-18. Balanced Amplifier Block Diagram.

PBN-88-1090

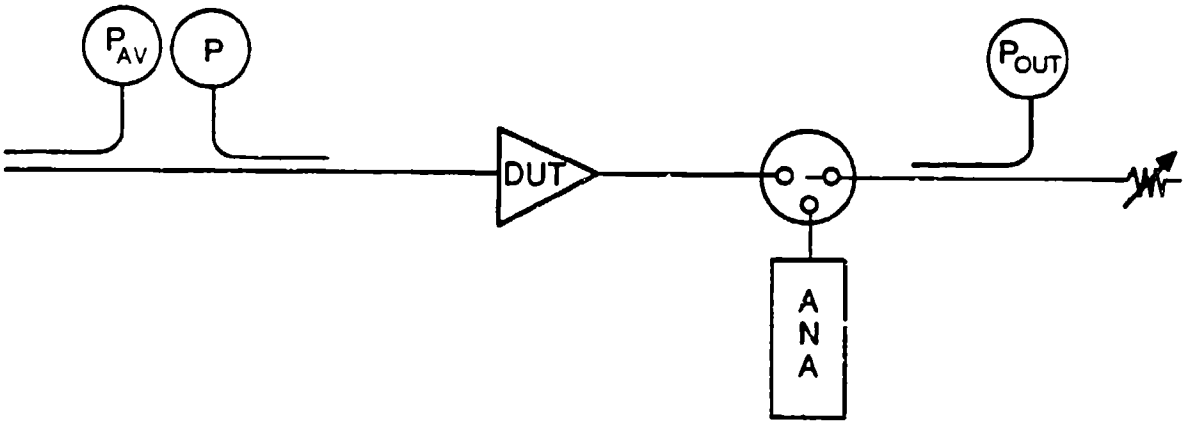

Figure 4-19. Load Pull Set-up.

PBN-88-1094

Load Pull Data

Transformed Max. Power Point to the Center of the Smith Chart

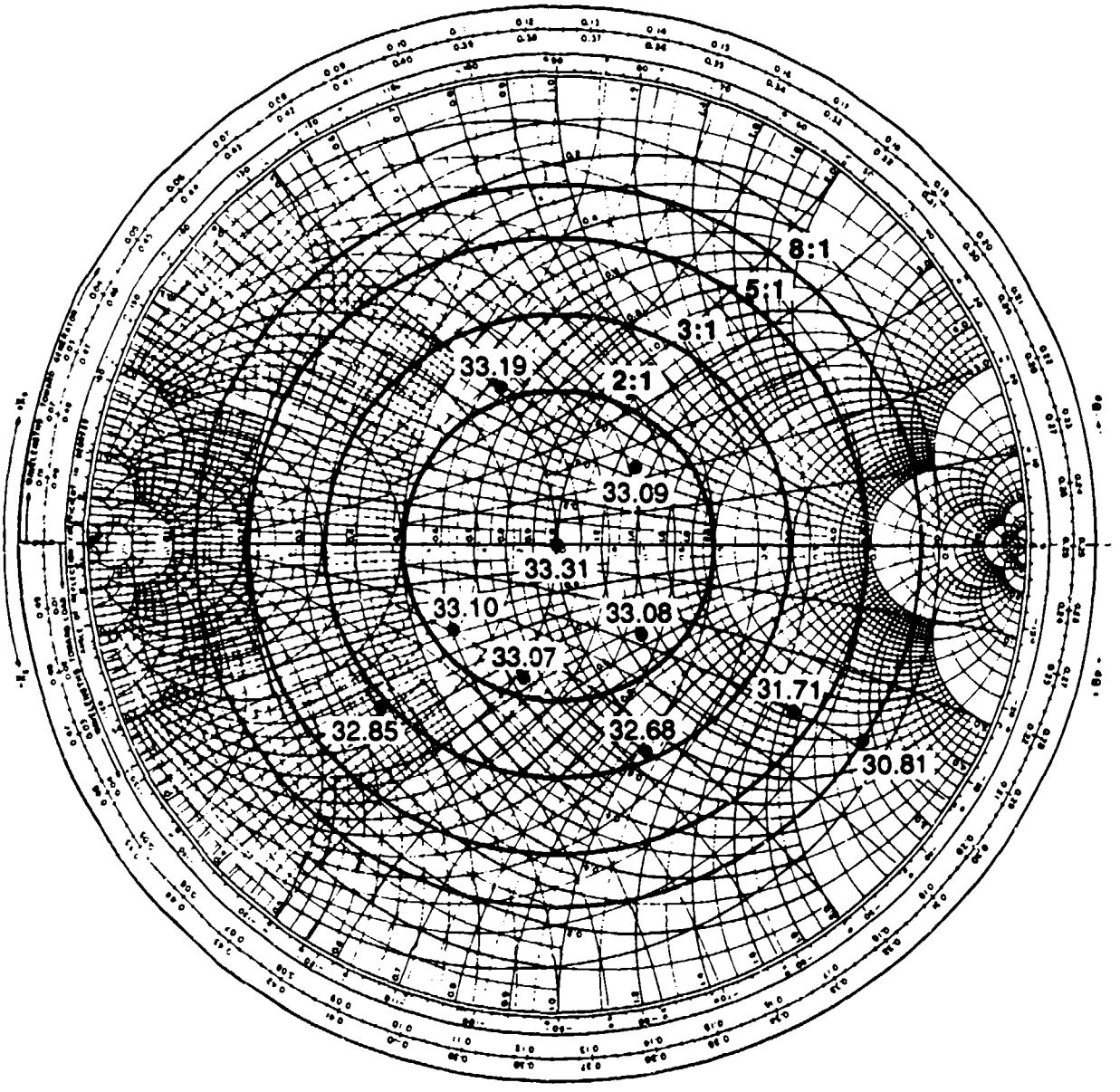

Figure 4-20. Load Pull Results.

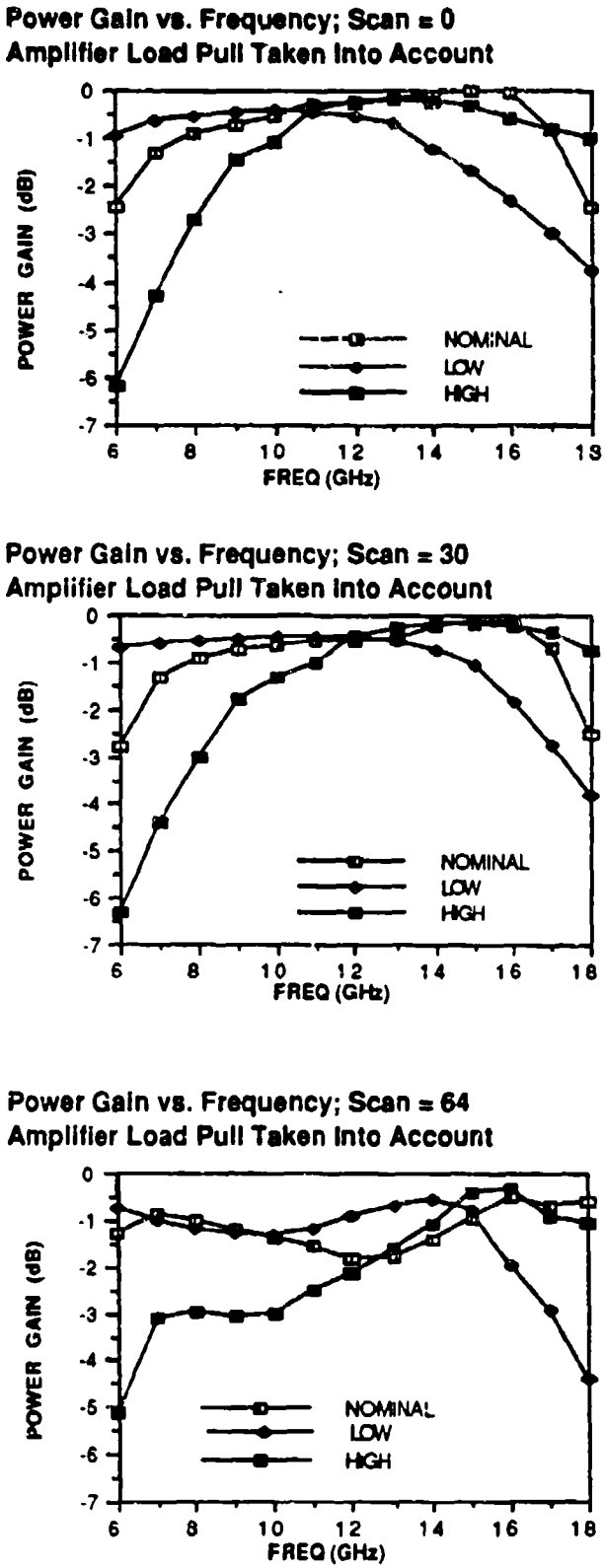

Figure 4-21. Notch Power Gain vs. Frequency with Load Pull Effects.

4.13 Slotline Termination Tuning Circuitry

In the interior regions of the array, fields are not tightly bound to the slot. Because of this, electronic displacement of the apparent notch short circuit plane cannot be achieved using single or multiple point diodes. It is necessary to continuously extend the electronic short over the length of slot to be terminated. This can be accomplished as shown in Figure 4-22. A 0.005" thick, 0.102" x 0.040" bulk silicon PIN diode is laid plane parallel to each slot of the radiator. The bulk diode is plated with bias grids in the fashion described by Mortenson, et al [2]. Bias grids on the ground plane side are shorted to the ground plane using plated through holes or pins. Bias grids away from the ground planes are connected to parallel dc bias lines etched on 0.005" thick Duroid. With this arrangement, the bias circuit and electromagnetic walls of the structure are coincident. Based on Mortenson's results, the bulk resistivity of the diode can be varied from 300 ohm-cm to 1 ohm-cm with a bias current of 56 mA per diode.

With the diodes conducting, the shorting pins and bulk diodes form a cavity which effectively displaces the notch short circuit plane to the aperture side of the diode. This occurs specifically due to the small spacing between notch radiators. Beyond the termination of the slotline, the array structure consists of square waveguides with a cut-off frequency of 24.9 GHz. In the region bounded by the conducting diodes, the cut-off frequency falls approximately to 24 GHz. Hence, the open structure of the unperturbed slot region is effectively terminated by below cut-off waveguides with small apparent recession of the shorting plane due to finite penetration of evanescent fields into the square guides (Appendix B).

The switching speed of the diode can be estimated as being of the order of the thickness of the intrinsic region divided by twice the drift velocity of the carriers [3,4]. Since the entire

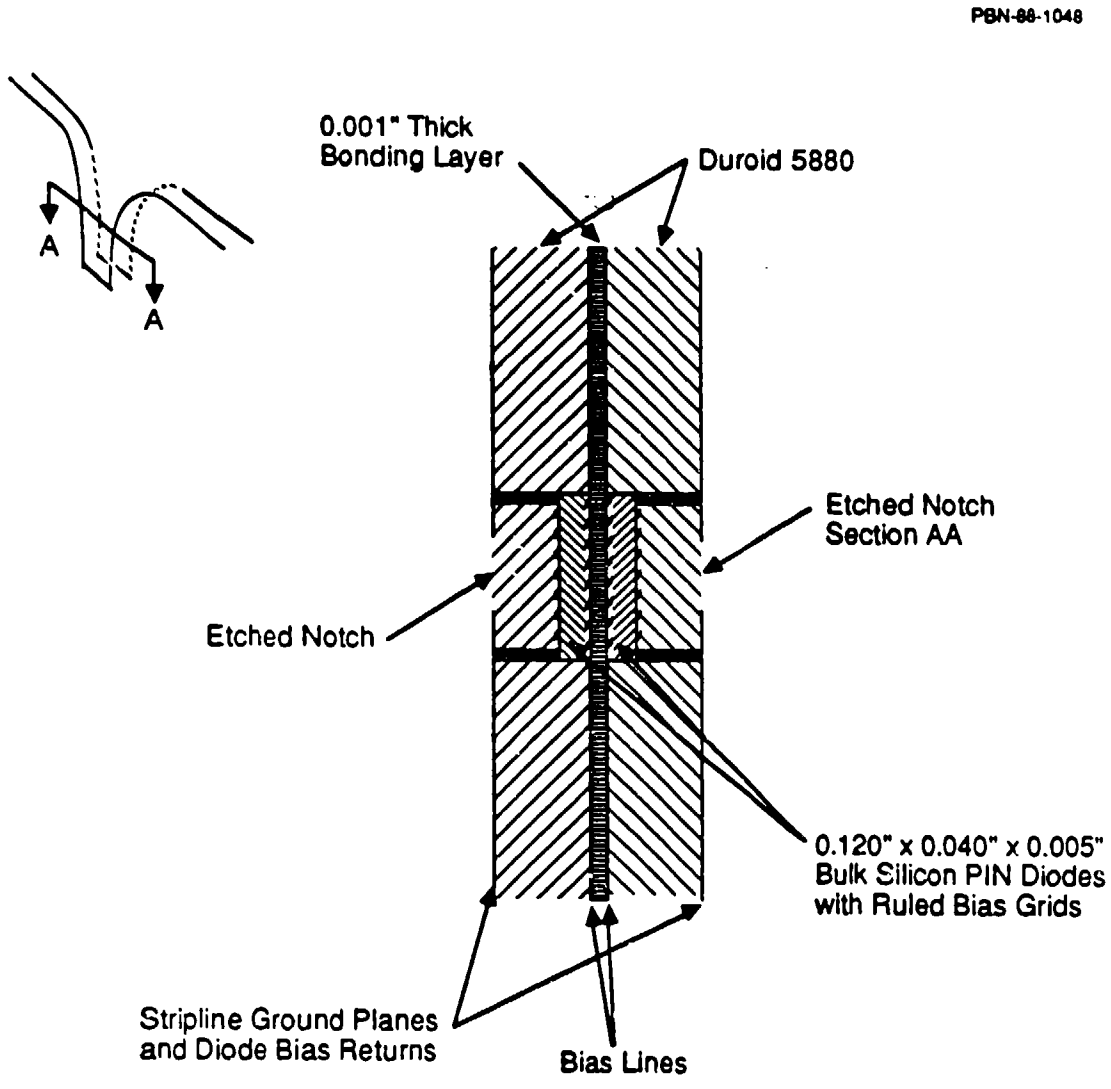

Figure 4-22. Electronic Notch Length Selection Switch.

diode is 0.005" thick, the intrinsic region of the diode must be less than 0.005" wide. Nonetheless, using 0.005" as the intrinsic region width and a saturation velocity of 1×10^7 cm/sec, the theoretical diode switching speed is less than 1 ns. A more realistic estimate of the diode switching speed is on the order of 50 ns. This indicates that the bulk diode switching speed should not limit the performance of the slotline tuning circuitry in the 6-18 GHz frequency band.

4.14 Slotline Tuned Radiator Performance

An estimate of electronically tuned radiator performance was obtained using methods outlined in Appendix B. For the cases studied, the diode loss in the conducting state (1 ohm-cm resistivity) reduced the radiated power by approximately 0.1 dB relative to a perfect notch short circuit. A very small improvement in VSWR was obtained. In the non-conducting state, the loss increase caused by the diode is approximately 0.1 dB. It is evident from these results that the bulk diode approach to notch length electronic switching does not significantly alter performance as defined by Figure 4-16.

5.0 CONCLUSION

An MMIC compatible mismatch compensation scheme for a notch radiator was developed. The compensation scheme tuned the notch radiator by electrically varying the radiator's stripline and slotline electrical lengths. With only two tuned states, the compensated radiator met the system bandwidth, VSWR, and scan angle requirements. The loss caused by the tuning circuitry was less than the improvement in system gain (at frequencies of high uncompensated notch input VSWR) and therefore the compensated radiator has improved performance over the "best case" uncompensated notch radiator in the 6-18 GHz frequency band.

The actual stripline tuning circuitry of an assembled compensated notch radiator will probably differ from what is presented in this report. A varactor was used as the stripline tuning device because it is a mature device and its capacitance and resistance had been determined at X-band frequencies. One limitation of a varactor is its relatively low power handling capability. A GaAs PIN diode, once it is sufficiently developed, would be a better stripline tuning circuit device due to its high power handling capability and its potential of low "on" resistance (less than a varactor "on" resistance). Since a GaAs PIN diode has the potential of lower loss than a varactor, our analysis represents a "worst-case" analysis. A compensated notch radiator using a PIN diode as the stripline tuning device should have improved performance over the compensated notch radiator presented herein.

The compensated notch was analyzed with minor variations in the physical dimensions of the stripline and slotline tuning circuitry (simulate manufacturing tolerances). Even with these tuning circuit variations, except at an isolated frequency and high scan angles, the compensated notch still met the system requirements. This indicates an insensitive compensation design that is producible.

Both the notch stripline and slotline lengths have to be varied in order to meet the VSWR specification over the 6-18 GHz frequency band. This nessesitates tuning circuitry on both the stripline and slotline which will require modification of the multilayer radiator substrate. The modification will involve opening layers of the substrate in order to place tuning devices on inner layers of the substrate. These additional fabrication steps will make the compensated notch more expensive to fabricate than an uncompensated notch. The added fabrication expense will yield a notch radiator with unprecedented performance that will directly result in improved antenna system performance.

6.0 REFERENCES

(1) Lawrence R. Lewis and Jerome Pozgay, "Broadband Antenna Study," Final Report, Contract no. F19628-72-C-0202, Raytheon Company, Missile Systems Division, March 1975.

(2) Kenneth E. Mortenson, Jose M. Borrego, Paul E. Bakeman, and Ronald J. Gutmann, "Microwave Silicon Windows For High-Power Broad-Band Switching Applications," IEEE Journal of Solid-State Circuits, vol. sc-4, no. 6, December 1969.

(3) G. Lucovsky, R. F. Schwarz, and R. B. Emmons, "Transit-Time Considerations in p-i-n Diodes," Journal of Applied Physics, vol. 35, no. 3, March 1964.

(4) S. M. Sze, "Physics of Semiconductor Devices," John Wiley and Sons, New York, 1981, page 117.

APPENDIX A
NOTCH INPUT VSWR DERIVATION

Applying lossless conditions (unitary properties);

Column 1

$$S_{11}S_{11}^{*} + S_{21}S_{21}^{*} + S_{31}S_{31}^{*} + S_{31}S_{31}^{*} = 1$$

$$\text{(A)}\quad |S_{11}|^2 + |S_{21}|^2 + 2|S_{31}|^2 = 1$$

Columns 1 and 2

$$S_{11}S_{21}^{*} + S_{21}S_{11}^{*} + S_{31}(-S_{31})^{*} + S_{31}(-S_{31})^{*} = 0$$

$$\text{(B)}\quad S_{11}S_{21}^{*} + S_{21}S_{11}^{*} - 2|S_{31}|^2 = 0$$

From (A) and (B)

$$|S_{11}|^2 + |S_{21}|^2 + S_{11}S_{21}^{*} + S_{21}S_{11}^{*} = 1$$

$$\left(S_{11} + S_{21}\right)\left(S_{11}^{*} + S_{21}^{*}\right) = 1$$

$$\left(S_{11} + S_{21}\right)\left(S_{11} + S_{21}\right)^{*} = 1$$

$$|S_{11} + S_{21}|^2 = 1$$

$$S_{21} = 1 - S_{11}$$

Column 3

$$\left(\bar{\eta}S_{31}\right)\left(\bar{\eta}S_{31}\right)^{*} + \left(-\bar{\eta}S_{31}\right)\left(-\bar{\eta}S_{31}\right)^{*} + S_{33}S_{33}^{*} + S_{43}S_{43}^{*} = 1$$

(A) $$2\bar{\eta}|S_{31}|^{2} + |S_{33}|^{2} + |S_{43}|^{2} = 1$$

Column 3 and 4

$$\left(\bar{\eta}S_{31}\right)\left(\bar{\eta}S_{31}\right)^{*} + \left(-\bar{\eta}S_{31}\right)\left(-\bar{\eta}S_{31}\right)^{*} + S_{33}S_{43}^{*} + S_{43}S_{33}^{*} = 0$$

(B) $$2\bar{\eta}|S_{31}|^{2} + S_{33}S_{43}^{*} + S_{43}S_{33}^{*} = 0$$

From (A) and (B)

$$1 - |S_{33}|^{2} - |S_{43}|^{2} = - S_{33}S_{43}^{*} - S_{43}S_{33}^{*}$$

$$|S_{43}|^{2} + |S_{33}|^{2} - S_{33}S_{43}^{*} - S_{43}S_{33}^{*} = 1$$

$$\left(S_{43} - S_{33}\right)\left(S_{43}^{*} - S_{33}^{*}\right) = 1$$

$$\left(S_{43} - S_{33}\right)\left(S_{43} - S_{33}\right)^{*} = 1$$

$$|S_{43} - S_{33}|^{2} = 1$$

$$S_{43} = 1 + S_{33}$$

When the stripline is open circuit terminated at $Y = y_2$ and the slit is short circuit terminated at $X = -x_2$, then at $Y = a/2$,

$$V_2^{+} = \vec{\Gamma} V_2^{-} e^{-\left(jk_{\varepsilon}(2y_2 - a)\right)} = \alpha V_2^{-}$$

and at $X = 0^{-}$,

$$V_3^{+} = -V_3^{-} e^{\left(2jk_{x_o}x_2\right)} = \beta V_3^{-}$$

The reflection coefficient in the expression for V_2^+ has a modulus 1 and phase slightly different than zero, corresponding to a small translation of the open circuit plane from the physical location of the termination (slight phase shift due to fringing capacitance).

Assuming the aperture is not matched;

V_4^+ is not equal to 0

$$V_4^+ = \Gamma_{ap} V_4^- e^{-2jk_x(D - X_2)} = \delta V_4^-$$

From the scattering matrix;

$$V_4^- = S_{31}V_1^+ - S_{31}V_2^+ + S_{43}V_3^+ + S_{33}V_4^+$$

$$V_4^- = S_{31}\left(V_1^+ - \alpha V_2^-\right) + S_{43}\beta V_3^- + S_{33}\delta V_4^-$$

$$V_4^-\left(1 - \delta S_{33}\right) = S_{31}\left(V_1^+ - \alpha V_2^-\right) + S_{43}\beta V_3^-$$

$$V_4^- = \frac{S_{31}\left(V_1^+ - \alpha V_2^-\right) + S_{43}\beta V_3^-}{1 - \delta S_{33}}$$

$$V_3^- = S_{31}V_1^+ - S_{31}V_2^+ + S_{33}V_3^+ + S_{43}V_4^+$$

$$V_3^- = S_{31}\left(V_1^+ - V_2^+\right) + S_{33}\beta V_3^- + S_{43}\delta\left[\frac{S_{31}\left(V_1^+ - \alpha V_2^-\right) + S_{43}\beta V_3^-}{1 - \delta S_{33}}\right]$$

$$V_3^- \left[1 - S_{33}\beta - \frac{S_{43}^2 \delta\beta}{1 - \delta S_{33}} \right] = S_{31} \left(V_1^+ - \alpha V_2^- \right) \left[1 + \frac{S_{43}\delta}{1 - \delta S_{33}} \right]$$

$$V_3^- \left[\frac{\left(1 - S_{33}\beta\right)\left(1 - \delta S_{33}\right) - S_{43}^2 \delta\beta}{1 - \delta S_{33}} \right] = S_{31} \left(V_1^+ - \alpha V_2^- \right)$$

(cont'd next line)

$$\left[\frac{1 - \delta S_{33} + S_{43}\delta}{1 - \delta S_{33}} \right]$$

$$V_3^- = \frac{S_{31} \left(V_1^+ - \alpha V_2^- \right) \left[1 - \delta S_{33} + S_{43}\delta \right]}{\left(1 - S_{33}\beta\right)\left(1 - \delta S_{33}\right) - S_{43}^2 \delta\beta}$$

$$V_3^- = \frac{S_{31} \left(V_1^+ - \alpha V_2^- \right) \left[1 - \delta S_{33} + S_{43}\delta \right]}{1 - \delta S_{33} - S_{33}\beta + \beta\delta S_{33}^2 - S_{43}^2 \delta\beta}$$

$$V_3^- = \frac{S_{31} \left(V_1^+ - \alpha V_2^- \right) \left[1 - \delta S_{33} + S_{43}\delta \right]}{1 - \delta S_{33} - \beta S_{33}\left(1 - \delta S_{33}\right) - \beta\delta S_{43}^2}$$

$$\text{Set } A = \frac{1 - \delta S_{33} + \delta S_{43}}{1 - \delta S_{33} - \beta S_{33}\left(1 - \delta S_{33}\right) - \beta\delta S_{43}^2}$$

$$V_3^- = A \left(V_1^+ - \alpha V_2^- \right) S_{31}$$

From before;

$$V_4^- = \frac{S_{31} \left(V_1^+ - \alpha V_2^- \right) + S_{43}\beta V_3^-}{1 - \delta S_{33}}$$

Substitute in V_3^-

$$V_4^- = \frac{S_{31} \left(V_1^+ - \alpha V_2^- \right) + S_{43}\beta \left[A \left(V_1^+ - \alpha V_2^- \right) S_{31} \right]}{1 - \delta S_{33}}$$

$$V_4^- = \frac{S_{31}\left(V_1^+ - \alpha V_2^-\right)\left[1 + A\beta S_{43}\right]}{1 - \delta S_{33}}$$

$$V_2^- = S_{21}V_1^+ + S_{11}V_2^+ - \bar{\eta}S_{31}V_3^+ - \bar{\eta}S_{31}V_4^+$$

$$V_2^- = S_{21}V_1^+ + S_{11}\alpha V_2^- - \bar{\eta}S_{31}V_3^- - \bar{\eta}S_{31}\delta V_4^-$$

$$V_2^- = S_{21}V_1^+ + S_{11}\alpha V_2^- - \bar{\eta}S_{31}\left[\beta\left(AS_{31}\left(V_1^+ - \alpha V_2^-\right) + \right.\right.$$

(cont'd next line)

$$\left.\left.\frac{\delta\left[S_{31}\left(V_1^+ - \alpha V_2^-\right)\left(1 + A\beta S_{43}\right)\right]}{1 - \delta S_{33}}\right)\right]$$

$$V_2^- = S_{21}V_1^+ + S_{11}\alpha V_2^- - \bar{\eta}S_{31}^2\left(V_1^+ - \alpha V_2^-\right)\left[\beta A + \frac{\delta\left(1+A\beta S_{43}\right)}{1 - \delta S_{33}}\right]$$

$$V_2^-\left(1 - S_{11}\alpha - \bar{\eta}S_{31}^2\alpha\left[\beta A + \frac{\delta\left(1 + A\beta S_{43}\right)}{1 - \delta S_{33}}\right]\right) = \text{(cont'd next line)}$$

$$V_1^+\left(S_{21} - \bar{\eta}S_{31}^2\left[\beta A + \frac{\delta\left(1 + A\beta S_{43}\right)}{1 - \delta S_{33}}\right]\right)$$

$$V_2^- = V_1^+\left[\frac{S_{21} - \bar{\eta}S_{31}^2\left[\beta A + \frac{\delta\left(1 + A\beta S_{43}\right)}{1 - \delta S_{33}}\right]}{1 - S_{11}\alpha - \bar{\eta}S_{31}^2\alpha\left[\beta A + \frac{\delta\left(1 + A\beta S_{43}\right)}{1 - \delta S_{33}}\right]}\right]$$

$$\text{Set } B = \frac{S_{21} - \bar{\eta}S_{31}^2\left[\beta A + \frac{\delta\left(1 + A\beta S_{43}\right)}{1 - \delta S_{33}}\right]}{1 - S_{11}\alpha - \bar{\eta}S_{31}^2\alpha\left[\beta A + \frac{\delta\left(1 + A\beta S_{43}\right)}{1 - \delta S_{33}}\right]}$$

$$V_2^- = BV_1^+$$

From before;

$$V_4^- = \frac{S_{31}\left(V_1^+ - \alpha V_2^-\right)\left[1 + A\beta S_{43}\right]}{1 - \delta S_{33}}$$

Substitute in V_2^-

$$V_4^- = \frac{S_{31}\left(V_1^+ - \alpha B V_1^+\right)\left[1 + A\beta S_{43}\right]}{1 - \delta S_{33}}$$

$$V_4^- = \frac{S_{31}\left(1 - \alpha B\right)\left[1 + A\beta S_{43}\right]V_1^+}{1 - \delta S_{33}}$$

From before;

$$V_3^- = A\left(V_1^+ - \alpha V_2^-\right)S_{31}$$

Substitute in V_2^-

$$V_3^- = A\left(V_1^+ - \alpha B V_1^+\right)S_{31}$$

$$V_3^- = AS_{31}\left(1 - \alpha B\right)V_1^+$$

$$V_1^- = S_{11}V_1^+ + S_{21}V_2^+ + \bar{\eta}S_{31}V_3^+ + \bar{\eta}S_{31}V_4^+$$

$$V_1^- = S_{11}V_1^+ + S_{21}\alpha V_2^- + \bar{\eta}S_{31}\beta A S_{31}\left(1 - \alpha B\right)V_1^+ + \bar{\eta}S_{31}\delta S_{31}$$

(cont'd next line)

$$\frac{\left(1 - \alpha B\right)\left[1 + A\beta S_{43}\right]V_1^+}{1 - \delta S_{33}}$$

$$V_1^- = S_{11}V_1^+ + S_{21}\alpha B V_1^+ + \bar{\eta}\beta A S_{31}^2\left(1 - \alpha B\right)V_1^+ + \bar{\eta}\delta S_{31}^2$$

(cont'd next line)

$$\frac{\left(1 - \alpha B\right)\left[1 + A\beta S_{43}\right]}{1 - \delta S_{33}} V_1^+$$

$$V_1^- = V_1^+\left[S_{11} + S_{21}\alpha B + \bar{\eta}S_{31}^2\left[1 - \alpha B\right]\left[\beta A + \frac{\delta\left(1 + A\beta S_{43}\right)}{1 - \delta S_{33}}\right]\right]$$

From before;

$$A = \frac{1 - \delta S_{33} + \delta S_{43}}{1 - \delta S_{33} - \beta S_{33}\left(1 - \delta S_{33}\right) - \beta\delta S_{43}^2}$$

Know $S_{43} = 1 + S_{33}$

$$A = \frac{1 - \delta S_{33} + \delta + \delta S_{33}}{1 - \delta S_{33} - \beta S_{33}\left(1 - \delta S_{33}\right) - \beta\delta\left(1 + 2S_{33} + S_{33}^2\right)}$$

$$A = \frac{1 + \delta}{1 - \delta S_{33} - \beta S_{33} + \beta\delta S_{33}^2 - \beta\delta - 2S_{33}\beta\delta - \beta\delta S_{33}^2}$$

$$A = \frac{1 + \delta}{1 - \delta S_{33} - \beta S_{33} - \beta\delta - 2\beta\delta S_{33}}$$

$$A = \frac{1 + \delta}{1 - \beta\delta - S_{33}\left(\delta + \beta + 2\beta\delta\right)}$$

where A is not a function of α

From before;

$$B = \frac{S_{21} - \bar{\eta}S_{31}^2\left[\beta A + \frac{\delta\left(1 + A\beta S_{43}\right)}{1 - \delta S_{33}}\right]}{1 - S_{11}\alpha - \bar{\eta}S_{31}^2\alpha\left[\beta A + \frac{\delta\left(1 + A\beta S_{43}\right)}{1 - \delta S_{33}}\right]}$$

Know $S_{21} = 1 - S_{11}$

$$B = \frac{1 - S_{11} - \bar{\eta}S_{31}^2\left[\beta A + \frac{\delta(1 + A\beta S_{43})}{1 - \delta S_{33}}\right]}{1 - S_{11}\alpha - \bar{\eta}S_{31}^2\alpha\left[\beta A + \frac{\delta(1 + A\beta S_{43})}{1 - \delta S_{33}}\right]}$$

Let $C = \bar{\eta}S_{31}^2\left[\beta A + \frac{\delta(1 + A\beta S_{43})}{1 - \delta S_{33}}\right]$

where C is not a function of α

Then,

$$B = \frac{1 - S_{11} - C}{1 - S_{1}\cdot\alpha - \alpha C}$$

$$\alpha B = \frac{1 - S_{11} - C}{\frac{1}{\alpha} - S_{11} - C}$$

From before;

$$V_1^- = V_1^+\left[S_{11} + S_{21}\alpha B + \bar{\eta}S_{31}^2\left(1 - \alpha B\right)\left[\beta A + \frac{\delta(1 + A\beta S_{43})}{1 - \delta S_{33}}\right]\right]$$

Substitute in αB

$$V_1^- = V_1^+\left(S_{11} + S_{21}\left(\frac{1 - S_{11} - C}{\frac{1}{\alpha} - S_{11} - C}\right) + \bar{\eta}S_{31}^2\left[1 - \left(\frac{1 - S_{11} - C}{\frac{1}{\alpha} - S_{11} - C}\right)\right]\right.$$

(cont'd next line)

$$\left.\left[\beta A + \frac{\delta(1 + S_{43}\beta A)}{1 - \delta S_{33}}\right]\right)$$

$$V_1^- = V_1^+\left[S_{11} + S_{21}\left(\frac{1 - S_{11} - C}{\frac{1}{\alpha} - S_{11} - C}\right) + C\left(1 - \left[\frac{1 - S_{11} - C}{\frac{1}{\alpha} - S_{11} - C}\right]\right)\right]$$

$$V_1^- = V_1^+ \left[S_{11} + S_{21} \left(\frac{1 - S_{11} - C}{\frac{1}{\alpha} - S_{11} - C} \right) + C \left(\frac{\frac{1}{\alpha} - S_{11} - C - 1 + S_{11} + C}{\frac{1}{\alpha} - S_{11} - C} \right) \right]$$

$$V_1^- = V_1^+ \left[S_{11} + S_{21} \left(\frac{1 - S_{11} - C}{\frac{1}{\alpha} - S_{11} - C} \right) + C \left(\frac{\frac{1}{\alpha} - 1}{\frac{1}{\alpha} - S_{11} - C} \right) \right]$$

$$V_1^- = V_1^+ \left[\frac{\frac{S_{11}}{\alpha} - S_{11}^2 - CS_{11} + S_{21} - S_{11}S_{21} - CS_{21} + \frac{C}{\alpha} - C}{\frac{1}{\alpha} - S_{11} - C} \right]$$

Know $S_{21} = 1 - S_{11}$

$$V_1^- = V_1^+ \left[\frac{\frac{S_{11}}{\alpha} - S_{11}^2 - CS_{11} + 1 - S_{11} - S_{11} + S_{11}^2 - C + CS_{11} + \frac{C}{\alpha} - C}{\frac{1}{\alpha} - S_{11} - C} \right]$$

$$V_1^- = V_1^+ \left[\frac{\frac{S_{11}}{\alpha} - 2S_{11} + \frac{C}{\alpha} - 2C + 1}{\frac{1}{\alpha} - S_{11} - C} \right]$$

$$\frac{V_1^-}{V_1^+} = \frac{\frac{S_{11}}{\alpha} - 2S_{11} + \frac{C}{\alpha} - 2C + 1}{\frac{1}{\alpha} - S_{11} - C} = \Gamma_{in}$$

Where from before;

C is not a function of α

APPENDIX B
ESTIMATION OF BULK DIODE EFFECTS

The bulk silicon PIN diodes are inserted in the structure of the notch radiator to produce electronic motion of the short circuit termination of the notch structure. Figure B-1 shows a side view of one radiator in a singly polarized egg-crate array of notch radiators with E-plane segmentation provided by metallic planes. A bulk diode is indicated by dashed outline. Only the unflared region of the notch is shown. As discussed in Section 4-12, diodes (in pairs) are physically located between the stripline ground planes. Bias return is provided by these ground planes via plated through holds or pins. Plane T is the physical location of the notch bottom.

A unit cell of the resulting infinite structure is formed as shown in Figure B-2. In regions between the array aperture and T, the periodicity of the structure, and enforced active boundary conditions govern the modal field characterization. To the right of T, in Figure B-1, the unit cell is a rectangular waveguide with dimensions (A-h)xB. For proper notch array design, this terminating region is below cut-off at all operating frequencies.

The characterization of the discontinuities at T and T_1 follows identical formalisms: therefore the formulation presented here refers generally to left of the plane of interest (hatted quantities) and to right of the discontinuity (unhatted). Continuity of electric field at the plane demands

$$\sum_{i=1}^{\infty} \hat{A}_i \underline{\hat{e}}_i \left(x,y\right) = \sum_{n=1}^{\infty} A_n \underline{e}_n \left(x,y\right) \qquad \text{(B-1)}$$

where the scalar quantities are field expansion coefficients with units of voltage, and the vector quantities (single underscore)

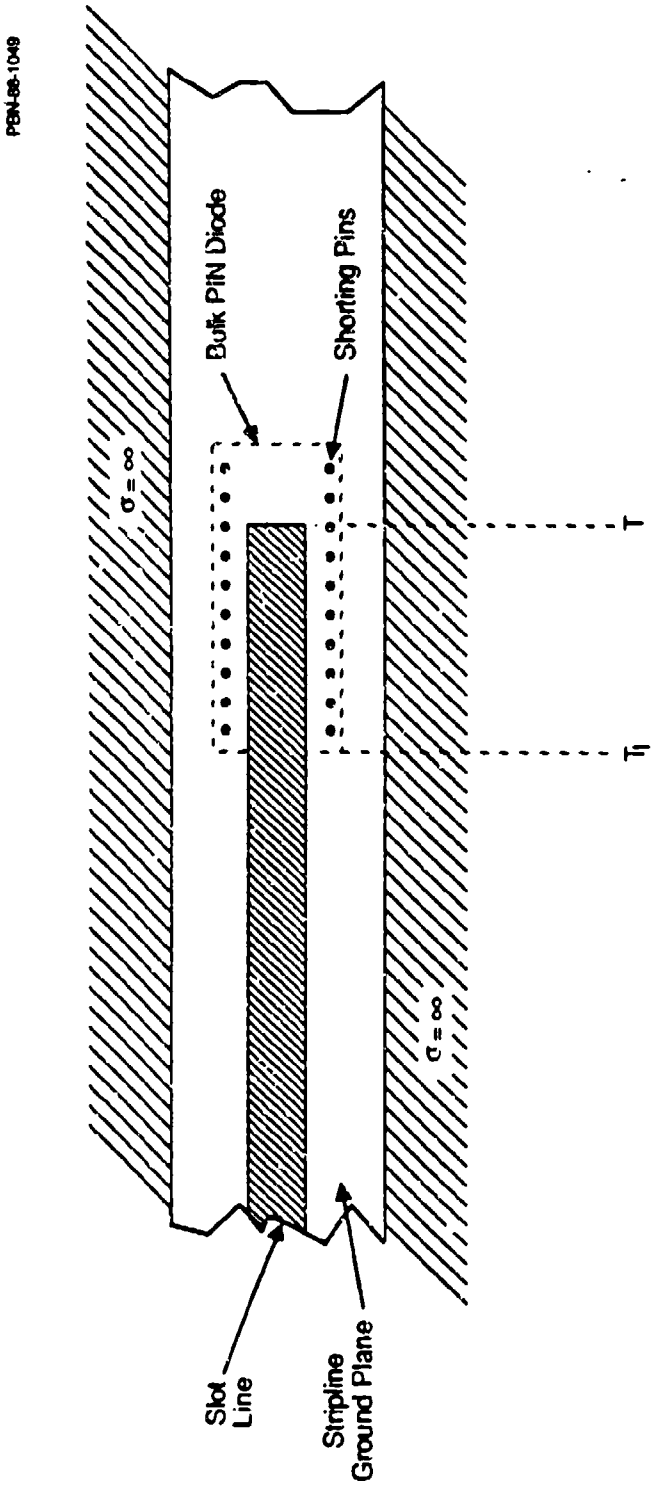

Figure B-1. Bulk PIN Diode Switched Notch Length.

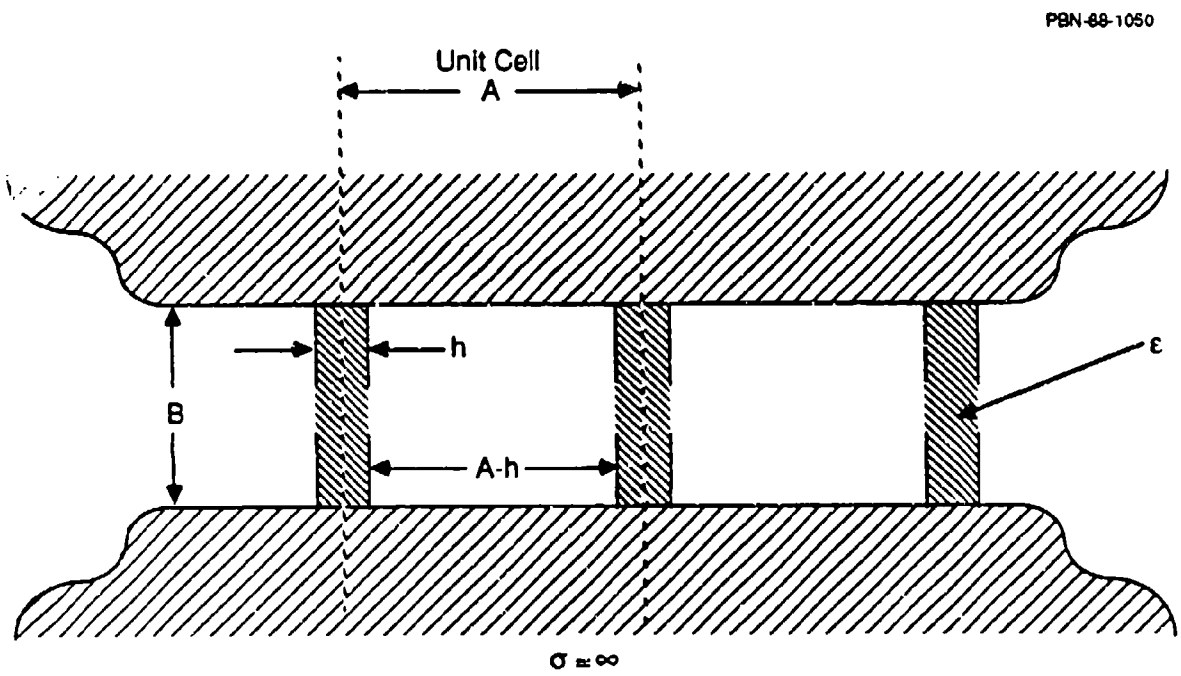

Figure B-2. Internal Unit Cell - Linear H-Plane Array of Notch Radiators.

are modal electric fields with units of inverse length. Equation (B-1) is valid over the entire discontinuity plane, by extension of domains of definition. In standard fashion, using a Galerkin procedure

$$\hat{A}_m = \sum_{n=1}^{\infty} A_n \xi_{mn} \tag{B-2}$$

where

$$\xi_{mn} = \int_{\text{cell}} dxdy \; \underline{e}_n \times \left(\underline{Z} \times \hat{\underline{e}}_m^*\right) \cdot \underline{Z} \tag{B-3}$$

and $\underline{Z}$ is a unit vector along the longitudinal guide direction. Truncating the modal representations to I and N modes, (B-2) can be rewritten in matrix notation as

$$\hat{\underline{A}} = \underline{\underline{\xi}} \underline{A} \tag{B-4}$$

Vector and matrix entities are obvious from comparison of equations (B-2) and (B-4).

Similarly, continuity of magnetic field produces

$$\underline{B} = \underline{\underline{\lambda}} \hat{\underline{B}} \tag{B-5}$$

where $\underline{B}$ and $\hat{\underline{B}}$ are modal magnetic field expansion coefficients in amperes, and the typical element of $\underline{\underline{\lambda}}$ is

$$\left[\underline{\underline{\lambda}}\right]_{nm} = \int_{\substack{\text{aperture} \\ \text{or} \\ \text{cell}}} dxdy \; \hat{\underline{e}}_m \times \left(\underline{Z} \times \underline{e}_n^*\right) \cdot \underline{Z} \tag{B-6}$$

The matrix $\underline{\underline{\lambda}}$ is obviously the conjugate-transpose of $\underline{\underline{\xi}}$.

$\underline{A}$, $\hat{\underline{A}}$, $\underline{B}$, and $\hat{\underline{B}}$ are total modal coefficients at the discontinuity plane (hence everywhere within the appropriate domain of definition). Let the superscripts + and - indicate incidence and reflection (reverse travel), respectively on the discontinuity plane. Then let

$$\underline{A} = \underline{V}^{+} + \underline{V}^{-}$$

$$\hat{\underline{A}} = \hat{\underline{V}}^{+} + \hat{\underline{V}}^{-}$$

(B-7a,b,c,d)

$$\underline{B} = \underline{I}^{+} + \underline{I}^{-} = \underline{\underline{Y}}_g\left(\underline{V}^{+} - \underline{V}^{-}\right)$$

$$\hat{\underline{B}} = \hat{\underline{I}}^{+} + \hat{\underline{I}}^{-} = \hat{\underline{\underline{Y}}}_g\left(\hat{\underline{V}}^{+} - \hat{\underline{V}}^{-}\right)$$

combining equations (B-4, B-5, B-7) and using $\underline{\underline{\lambda}} = \underline{\underline{\xi}}^{*t}$ gives

$$\hat{\underline{V}}^{-} = \left(\underline{\underline{1}} - \underline{\underline{\xi}}\,\underline{\underline{Z}}_g\,\underline{\underline{\xi}}^{*t}\hat{\underline{\underline{Y}}}_g\right)^{-1}\left[-\left(\underline{\underline{1}} + \underline{\underline{\xi}}\,\underline{\underline{Z}}_g\,\underline{\underline{\xi}}^{*t}\hat{\underline{\underline{Y}}}_g\right)\hat{\underline{V}}^{+} + \left(\underline{\underline{1}} + \underline{\underline{\xi}}\right)\underline{V}^{+}\right]$$

(B-8a,b)

$$\underline{V}^{-} = \left(\underline{\underline{Y}}_g - \underline{\underline{\xi}}^{*t}\hat{\underline{\underline{Y}}}_g\underline{\underline{\xi}}\right)^{-1}\left[-2\underline{\underline{\xi}}^{*t}\underline{\underline{Y}}_g\hat{\underline{V}}^{+} + \left(\underline{\underline{Y}}_g + \underline{\underline{\xi}}^{*t}\underline{\underline{Y}}_g\underline{\underline{\xi}}\right)\underline{V}^{+}\right]$$

Equations B-8a,b are the formal solution at each discontinuity. If the region to the right is below cut-off, or substantially so, then $\underline{V}^+ \sim \underline{0}$, and simultaneous solution of equations (B-7) gives

$$\hat{\underline{V}}^- = \left[2\underline{\xi}\left(\underline{\xi}^{*t}\hat{\underline{Y}}_g\underline{\xi} + \underline{Y}_g\right)^{-1}\underline{\xi}^{*t}\underline{Y}_g - \underline{1}\right]^{-1}\hat{\underline{V}}^+ \qquad \text{(B-9)}$$

To better appreciate equation (B-9), a single mode can be assumed in each region as an heuristic device. With this specialization,

$$\hat{V}_1^- = \frac{j|Z_{g1}||\xi_{11}|^2 - \hat{Z}_{g1}}{j|Z_{g1}||\xi_{11}|^2 + \hat{Z}_{g1}} \qquad \text{(B-10)}$$

Equation (B-10) is immediately recognized (in form) as the reflection coefficient of a propagating wave terminated in a beyond cut-off structure.

For the diode switched notch radiator, the dominant modes in the diode loaded and free regions are TE with respect to Z. Hence, if Y1 is the wavenumber in the diode free region, and Y1 is the wavenumber in the diode loaded region when the diode is conducting, then equation (B-10) can be rewritten as

$$\Gamma = \frac{j\left(\hat{\gamma}_1/|\gamma_1|\right)|\xi_{11}|^2 - 1}{j\left(\hat{\gamma}_1/|\gamma_1|\right)|\xi_{11}|^2 + 1} \qquad \text{(B-11)}$$

Hence if $\gamma 1$ and $\gamma 1$ are known, a first order approximation to the loss induced by the diode is obtained by replacing the short circuit termination of the stripline notch junction by the reflection coefficient in (B-11).